VALIDATION OF NEQUICK MODEL USING IONOSONDE OVER EAST AFRICA LONGITUDE SECTOR

By

KEBEDE BEKELE MAMO

SUBMITTED IN PARTIAL FULFILLMENT OF THE
REQUIREMENTS FOR THE DEGREE OF
MASTER OF SCIENCE IN PHYSICS
AT
ADDIS ABABA UNIVERSITY
ADDIS ABABA, ETHIOPIA
JUNE 2015

ADDIS ABABA UNIVERSITY
COLLEGE OF NATURAL SCIENCES
DEPARTMENT OF PHYSICS

The undersigned hereby certify that they have read and recommend to the School of Graduate Studies for acceptance a thesis entitled "**VALIDATION OF NEQUICK MODEL USING IONOSONDE OVER EAST AFRICA LONGITUDE SECTOR** " by **KEBEDE BEKELE MAMO** in partial fulfillment of the requirements for the degree of **Master of Science in Physics**.

Dated: June 2015

Supervisor:

Prof. Gizaw Mengistu Tsidu
(Botswana International University of Science and Technology/ Addis Ababa University)

Examiners:

Prof. A.V Gholap

Dr. Gebregeworgs Abraha

ADDIS ABABA UNIVERSITY

Date: **June 2015**

Author: **KEBEDE BEKELE MAMO**

Title: **VALIDATION OF NEQUICK MODEL USING IONOSONDE OVER EAST AFRICA LONGITUDE SECTOR**

Department: **Physics**

Degree: **M.Sc.** Convocation: **June** Year: **2015**

Permission is herewith granted to Addis Ababa University to circulate and to have copied for non-commercial purposes, at its discretion, the above title upon the request of individuals or institutions.

Signature of Author

To my parents, sisters, brothers and relatives

Table of Contents

List of Figures

Acronyms

CCIR	Consulative Committe International Radio
CGM	Corrected Geomagnetic Coordinate
CODE	Center for Orbit Determination in Europe
DGR	Di Giovanni and Radicella
EDP	Electron Density Profile
EGNOS	European Geostationary Navigation Overlay Service
EUV	Extreme Ultraviolet
FORTRAN	FORmula TRANslation
GPS	Global Positioning System
HF	High Frequency
ICTP	International Center for Theoretical Physics
IGAM	Institute for Geophysics, Astrophysics and Meteorology
IGRF	International Geomagnetic Reference Field
ITU-R	International Telecomminucation Union Radiocomminucation
LF	Low Frequency
MF	Maximum Frequency
MHD	Magneto Hydro Dynamics
RF	Radio Frequency
RMSD	Root Mean Square Deviation
SID	Sudden Ionospheric Disturbance
STEC	Slant Total Electron Content

TEC	Total Electron Content
UT	Universal Time
VHF	Very High Frequency
VLF	Very Low Frequency

Abstract

An empirical electron density model, quick-run ionospheric electron (NeQuick), has been selected for the modelling of the ionospheric electron density profile. NeQuick ionospheric electron density model produces the full electron density profile in the ionosphere. The electron density profiles (EDP) from NeQuick model before and after ingestion of the ionosonde key parameters (foE, hmE, foF2 and hmF2) have been compared with ionosonde electron density profile for bottom side ionosphere from HF-viper radar installed at Welmera site. The comparisions show that the NeQuick model after ingestion of key parameters from ionosonde generally agrees well with the ionosonde observation. The root mean square deviation (RMSD) and correlation coefficient (R) for the two data sets are computed for the selected time. The RMSD of the NeQuick model after ingestion of ionosonde key parameters are lower than those values before ingestion of ionosonde key parameters. The computed correlation coefficients (R) also show an existence of stronger relationship after ingesting ionosonde key parameter values than those values before ingesting ionosonde key parameter values.

Acknowledgements

I wish to extend my sincere gratitude to my advisor, Prof. Gizaw Mengistu, for his guidance, motivation and continued support throughout the entire period of this study. I would like to thank the Aeronomy and Radiopropagation Laboratory of the Abdus Salam International Centre for Theoretical Physics (ICTP) in Trieste, Italy for making NeQuick model freely available on the web. I am highly indebted with all physics Departement staff and Dr Belayneh Mesfin, the head of physics Department , for the opportunity they gave me to utilize research logistics. Special thanks to Dr. Gebregeworgs Abraha for his bright experience sharing on all space courses and on my work and to w/ro Tsilat Adnew the secretary of physics department for kind cooperation. I am grateful to acknowledge Ambo University, for the consistent research fund support, which was crucial to the successful completion of this project. A special thanks goes to my Mum, Dad, brothers and sisters for their continuous love, care and support. I would like to also thank all my friends who have shown support in a number of ways.

Above all, I am most thankful to the Almighty God. He was the major source of strength throughout the project. It is an honor for me to express my deepest gratitude for keeping me under His grace for all this time.

Chapter 1

Introduction

The ionosphere is the region of partially ionized plasma above the Earth's atmosphere formed due to primarily photoionization of the neutral atoms and molecules. The increase in the density of the atmosphere as we go further down to the surface of the Earth and the decrease in the intensity of photons as it bombards the neutral atoms and the availability of different atoms and molecules at different heights from the Earth's surface forms a large scale vertical layer of ionization with the ionosphere. This makes the ionosphere to exist as vertically stratified partially ionized plasma state from at about 60 km–1000 km from the surface of the Earth [1, 2]. The ionosphere affects the propagation of electromagnetic waves passing through it [3]. As radio wave penetrate the ionosphere their refractive index is a function of the waves frequency, the electron density and to a small extent the Earth's magnetic field. This means the ionosphere is a dispersive medium for the propagation of electromagnetic waves.

Looking back on this century's development of knowledge about the ionosphere we can see the development of instrumentation which created the data necessary for understanding of the ionosphere. One important instrument is the ionosonde, that is a radio sounder which sweeps through a large range of frequencies, recording the range of echoes reflected from the ionosphere to produce ionograms. Ionograms are recorded tracings of reflected high frequency radio pulses generated by an ionosonde. Unique relationships exist between the sounding frequency and the ionization densities which can reflect it. As the sounder sweeps from lower to higher frequencies, the signal rises above the noise of commercial radio sources and records the return signal reflected from the different layers of the ionosphere. These echoes form characteristic patterns of "traces" that comprise the ionogram. Radio pulses travel more slowly within the ionosphere than in free space, therefore, the apparent or "virtual" height is recorded instead of a true height. For frequencies

approaching the level of maximum plasma frequency in a layer, the virtual height tends to infinity, because the pulse must travel a finite distance at effectively zero speed. The frequencies at which this occurs are called the critical frequencies. Characteristic values of virtual heights (designated as h'E, h'F, and h'F2, etc.) and critical frequencies (designated as foE, foF1, and foF2, etc.) of each layer are scaled, manually or by computer, from the ionograms.

To describe the electron density of the ionosphere, the NeQuick model uses a DGR profile formulation, which is proposed by di Giovanni and Radicella, 1990 [4]. The NeQuick is an ionospheric electron density model developed at the Aeronomy and Radio propagation Laboratory of the Abdus Salam International Centre for Theoretical Physics (ICTP), Trieste, Italy, and at the Institute for Geophysics, Astrophysics and Meteorology (IGAM) of the University of Graz, Austria. It allows calculating the electron concentration at any given location in the ionosphere and thus the Total Electron Content (TEC) along any ground to satellite ray-path by means of numerical integration. The basic inputs are: position, time and solar flux (or sunspot number) and the output is the electron concentration at a given location in space and time. The model describes the ionosphere separately for the bottomside and the topside. The bottomside goes from 60 km to the F2-layer peak and consists of a sum of five semi-Epstein layers. The topside is above the F2 peak layer and it is described by means of a semi-Epstein layer with a height-dependent thickness parameter. To compute the thickness parameters and the peak electron density and height for the Epstein layers, NeQuick employs the ionosonde parameters which can be modeled or experimentally derived.

The thesis comprises of seven Chapters. Chapter 1 covers a brief introduction of the thesis. Chapter 2 is about the Earth's ionosphere with discussions on the formation, layers, disturbances and propagation of electromagnetic waves in the ionosphere. Chapter 3 gives the description of the vertical ionospheric sounding, ionosonde radar and the ionogram. A brief description of the model used in this thesis is given in Chapter 4. This chapter presents the development of the model and parameters used, as well as the capabilities of the model. Chapter 5 describes various data and methodologies used in this thesis. Chapter 6 provides results and discussions. Finally, conclusion of the thesis is presented in the seventh Chapter.

Chapter 2

The Ionosphere

2.1 Introduction

Balfour Stewart was the first person to postulate an ionosphere when, in 1882, he attributed currents in the upper atmosphere as the probable origin of the electric currents that produced the solar controlled variation in the Earth's magnetic field measured at the Earth's surface [2]. According to Kelley [1], the discovery of the ionosphere came from radio wave observations and the recognition that only a reflecting layer composed of electrons and positive ions could explain the characteristics of the data. The term ionosphere was first used by Sir Robert Watson-Watt in a letter to the secretary of British Radio Research Board in 1926 [5]. The expression came into wide use during the period 1932-34 when Watson-Wat, Appleton, Radcliff and others used it in papers and books [5]. Today, radio science remains the primary tool for obtaining measurements of the ionosphere. Using short vertically directed radio frequency pulses and inferring the height of electrically reflecting layer from timing the arrival of the reflecting signal is still used in sounding the ionosphere [2].

2.2 The ionosphere of the Earth

The Earth's ionosphere, that covers to an altitude range of approximately 60km–1000 km, is historically the region of the atmosphere that affects the propagation of radio waves [6]. One may also define the Earth's ionosphere as the region of the Earth's upper atmosphere partially ionized due to primarily ultraviolet radiation from the Sun. Although

the ionosphere becomes sensible at about 50km from the surface of the Earth, its upper boundary is not well defined since it can be interpreted as the electron densities thinning into the plasmasphere (or protonosphere) and subsequently to the interplanetary plasma [5]. But the most important contribution for the ionosphere lies in the 90km–1000 km region from the surface of the Earth [6]. Most planets in the solar system do have their own ionosphere provided they have their own neutral gas-envelope (atmosphere) [1].

2.3 Formation of the ionosphere

The main distinction between the ionospheric region and other regions of the atmosphere is that the former contains more charged particles. The formation of the ionosphere depends on the activities of the Sun, because the solar extreme ultraviolet (EUV) light and X-ray radiation from the Sun are the main sources of plasma and energy for the ionosphere. The process by which the EUV light and X-ray radiation from the Sun interact with neutral atoms giving rise to free electrons is called photoionization. Because of this process, the ionosphere consists of free electrons and ions (see Fig. 2.1).

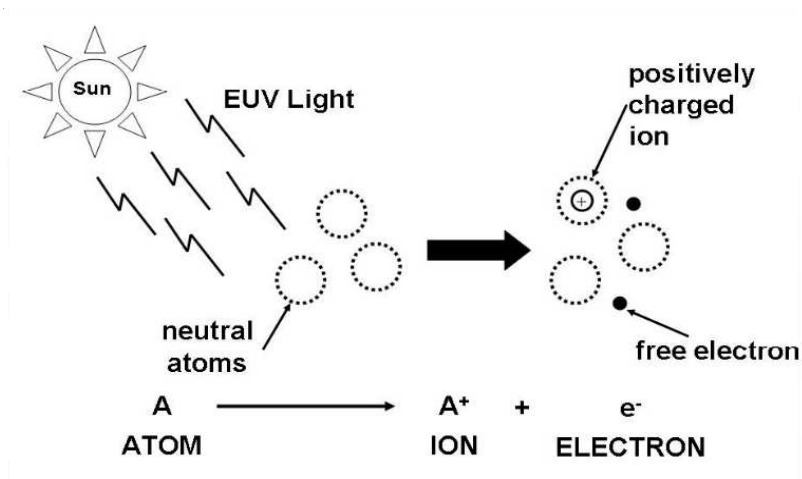

Figure 2.1: A representation of the photo ionization process due to the sun's extreme ultra violet (from[7]).

The net value of the number of free ions and electrons in the ionosphere is determined by the rate at which specific species of ions combine with electrons to form neutral atoms. This process is known as recombination and it occurs in two stages [7]:

- **Radiative recombination**:- This is the process whereby electrons combine directly with positively charged ions, converting them into neutral atoms and emitting a photon to conserve energy and momentum:

$$O^+ + e^- \longrightarrow O + photon \tag{2.3.1}$$

- **Dissociative recombination**:- This process occurs in two stages:
  In the first stage the positive ions (e.g., N^+) which are formed during the photoionization process interact with a neutral atom forming a positively charged molecular ion:

$$N^+ + O_2 \longrightarrow NO^+ + O \tag{2.3.2}$$

  In the second stage the electrons combine again with a positively charged ion (NO^+) to produce two neutral atoms:

$$NO^+ + e^- \longrightarrow N + O \tag{2.3.3}$$

Dissociative recombination is a faster mechanism than radiative recombination to loose electrons from the ionosphere. During sunset, the recombination process ceases, which results in a gradual drop in electron density as night progresses. Electron density is at its greatest during the middle of the day when photoionization is high. Because different gas atoms and molecules are more abundant in some regions of the neutral atmosphere than others, ionization and recombination of different species result in a different electron density distribution within different layers of the ionosphere. These layers are called D, E, F1 and F2 and are discussed in the next section.

2.4 Layers of the ionosphere

The decrease in light intensity and increase in neutral density with decrease in altitude forms an ionization peak in the ionosphere. However, due to the availability of different atoms and molecules with differing rates of absorption, the ionosphere at all latitudes has a tendency to separate into layers. However, a series of distinct regions or layers of electron density exist in the daytime ionosphere at mid-latitudes [1, 5]. These layers are denoted by the letters D, E, F1, and F2 (see Fig. 2.2). Each layer is generally characterized by a density maximum at a certain altitude and a density decrease with altitude on both sides of the maximum. According to the chemical composition ionosphere is also divided into regions at the different altitudes. These regions are; lower ionosphere (between about 50 km and 90 km), bottomside ionosphere (between about 90 km and 350 km) and the topside ionosphere (above about 350 km). The four layers are collectively known as bottomside ionosphere. Peak electron density of the ionosphere occurs usually at the F2 layer and the region above this layer is said to be topside ionosphere. There is a minimum frequency of an electromagnetic wave that can penetrate an ionospheric layer. This frequency is called the critical or plasma penetration frequency of the particular layer and it is denoted by foD, foE, foF1, and foF2 according to the designation of the ionospheric layers. The square of a critical frequency is linearly proportional to the maximum electron density of the individual layer and these are denoted by NmD, NmE, NmF1 and NmF2 respectively. Below about 90 km, in the lower ionosphere, measurements are made using Ground based ionosondes. Vertical sounding radar are used for recording the bottomside ionosphere, and satellite bourne ionosondes (topside sounders) are used for measuring the topside.

2.4.1 D layer

The D-layer is the lowest layer and lies between 60 and 90 km above the surface of the Earth. It is ionized during the day (mostly at noon) and quickly deionizes at night. The ionization is caused by solar X-ray radiation or Lyman alpha-hydrogen from the Sun. This lower layer absorbs the lower frequencies (below 10 MHz) and allows the higher frequencies to pass to outer layers. It is only present during the day, reducing and disappearing as the Sun sets. It may, however, sometimes remain due to the ionization effect of galactic cosmic rays [8]. At the lower level of this layer, the density of electrons is very high and the recombination of ionized particles occurs rapidly. It is important for radio propagation because (a) it absorbs energy from waves at Maximum Frequency (MF), High Frequency

(HF) and Very High Frequency (VHF), and (b) it reflects Low Frequency (LF) and Very Low Frequency (VLF) waves.

2.4.2 E layer

The E-layer lies above the D-layer and is found between about 90 and 150 km above the surface of the Earth. It is ionized during the day and the ionization process does not last long. The photoionization and recombination processes occur more slowly in the E-layer than in the D-layer. The former plays an important role in the quality of radio communication and radio waves, in that it refracts HF waves that would penetrate the D-layer. The charged particles in the E-layer are the results of ionization of molecular Oxygen (O_2) generated by soft X-rays as well as EUV radiation. Therefore the E-layer can reflect radio waves with frequencies lower than 10 MHz. At night this layer begins to disappear because the primary source of ionizationis no longer present.

2.4.3 F1 layer

The F1-layer is situated below the F2 layer and lies between 150 and 250 km above the surface of the Earth. At altitudes below and above this range, ions are lost from this layer due to recombination and attachment processes. The ionization of atoms such as Oxygen (O_2) and Nitrogen (N_2) occurs by Lyman Continuum or He emission and disappears after sunset. During the night the F1-layer quickly loses its ionization and disappears. There are certain conditions whereby the F1-layer is not present at all [7]. In particular, this layer is never present at night. It is rarely found in winter but is likely to appear during daytime in summer when the solar zenith angle is small and hence the peak altitude of ionization is lower [9]. The F1-layer is likely to appear during solar minimum periods when the rate of ionization is low and the transition altitude between molecular and atomic ions is higher.

2.4.4 F2 layer

The F2 layer lies between about 250 and 400 km, and is the uppermost layer of the bottomside ionosphere. Ionization in this layer occurs due to the photoionization of atomic oxygen by extreme EUV solar radiation from the Sun. This layer is very thick, more active and more highly ionized, but its ionization decreases during and after sunset.

Since F2 layer is the highest layer of the ionosphere, it consists of a greater concentration of free electrons and ions. It is the most important layer for HF radio propagation because:

- It is the only layer that survives at night and is present 24 hrs of the day;
- It reflects the radio waves needed for high frequency communication and broadcasting; and
- Its high altitude allows the longest distance and communication paths.

The variation of the ionospheric electron density with altitude is dependent on the different molecules that are dominant in a specific range of altitudes. Because the neutral gas density decreases with height, there are fewer neutral atoms allowed to participate in the ionization process at higher altitudes. The radiation intensity also increases at a lower altitude. Since the ionization appears differently at different ionospheric levels, it produces layers or regions which may be identified by their interaction with radio waves.

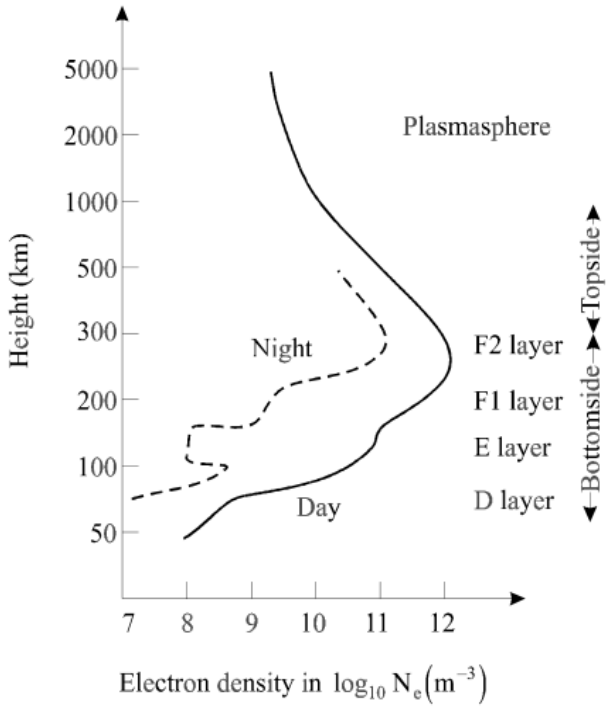

Figure 2.2: Vertical profiles of ionospheric electron density showing the distinct layers (from[5])

2.5 Ionospheric disturbances

2.5.1 Ionospheric storms

At different times the ionosphere suffers major perturbations called storms. They last from a few hours to a few days and tend to occur during times of geophysical disturbance resulting from increases in solar activity communicated via the solar wind. Three phases are identified in ionospheric storm. The first, known as initial or positive phase, is associated with an increase in electron density from the normal value and usually lasts for a few hours. Then follows the main or negative phase when the electron density are reduced below normal values. The final phase is the recovery phase in which the ionosphere gradually returns to normal over a period of one to several days [10].

2.5.2 Geomagnetic storms

Geomagnetic storms usually occur in conjunction with ionospheric storms and can be caused by solar flares, high speed solar wind stream and sudden disappearing filaments. The storms are usually associated with increased electron densities in the lower ionosphere and a simultaneous increase in absorption of radio waves. Like the ionospheric storm, it may last from a few hours to several days and it often exhibits three phases. A geomagnetic storm usually starts with an increase in the Earth's geomagnetic field intensity called the initial phase followed by a large decrease termed the main phase. Because magnetic storms can be monitored without great difficulty using a magnetometer, and long runs of such measurements exist, the magnetic storm has come to be a common reference point in geophysical studies [10].

2.5.3 Ionospheric scintillation

Small-scale structures in the electron content of the ionosphere can range from a few meters to a few kilometers in extent which can cause both refraction and diffraction effects on the electromagnetic waves propagating through the ionosphere. Consequently, the wavefront becomes crinkled giving rise to amplitude and phase fluctuations of the signal. These fluctuations lead to fading in signal power caused by small scale ionospheric structures are called ionospheric scintillations. Scintillation is more prevalent at very high and very low latitudes.

2.6 Variations of the ionosphere

The ionosphere is not a stable medium that allows the use of the same frequency throughout the year, or even over 24 hours. The ionosphere naturally varies with time of day, season and geographic position. The following major variation are discussed in brief.

2.6.1 Diurnal variation

The day and night electron density of the ionosphere is not the same. Night time electron densities are much lower than day time electron density because in night time the recombination rates are higher in the absence of ionization sources. The day time electron density reaches its peak value at noon hours. The main consituents of the ionsphere are neutral atoms and molecules. However, the charged nature of the ionosphere is due to the production of electrons and ions primarily by solar ultraviolet radiation from the sun. This again means that the ionosphere is produced during the day and is reduced during the night due to recombination processes of electrons and ions. Ionization depends primarily on the Sun and its activity. The amount of ionization in the ionosphere varies greatly with the amount of radiation received from the Sun.

2.6.2 Seasonal variation

The ionosphere exhibits strong seasonal and solar cycle variations because the main source of ionization and energy for the ionosphere is photo-ionization. Therefore, whenever there is a change in solar zenith angle or the solar radiation fluxes, the ionosphere will change. The ionospheres seasonal variation is related to a solar zenith angle change, while its solar cycle variation is related to a change in the solar EUV and X-ray radiation fluxes. However, the ionospheric variations are not always simple because the ionosphere is closely coupled to the thermosphere, which also undergoes seasonal and solar cycle changes.

2.6.3 Latitudinal variations

The ionosphere differs over the Earth from one place to the other. This is due to variations of the solar zenith angle. The solar zenith angle is the angle between the local zenith and the line of sight to the Sun. It describes the position of the Sun with respect to the zenith angle. Therefore the ionosphere has considerable variation with latitude.

2.7 Propagation of electromagnetic wave in the ionosphere

Ionosphere physics is related to plasma physics because the ionosphere is, of course, a weak natural plasma: an electrically neutral assembly of ions and electrons. The most important feature of the ionosphere is to reflect the radio waves up to 30 MHz. Especially, the propagation of radio waves in the HF band makes the necessary knowing the features and the characteristics of the ionospheric plasma media. Because, when the radio waves reflect in this media, they are reflected and refracted depending on their frequency, the frequency of the electrons in the plasma and the refractive index of the media and thus, they are absorbed and reflected by the media [8]. Ionospheric effect on electromagnetic waves, such as GPS signals, cannot be described by a simple dispersion. To describe the behavior of radio waves in the ionosphere we need to realize that the ionosphere is a partially ionized, spherically stratified plasma with irregularities upon which imposed a uniform magnetic field. That is we can treat the ionosphere as a plasma embedded in an electromagnetic field [11]. The four Maxwells equations in the plasma fluid can be written as

$$\vec{\nabla} \cdot \vec{E} = \frac{\rho}{\epsilon_0} \tag{2.7.1}$$

$$\vec{\nabla} \times \vec{E} = -\frac{\partial \vec{B}}{\partial t} \tag{2.7.2}$$

$$\vec{\nabla} \cdot \vec{B} = 0 \tag{2.7.3}$$

$$\vec{\nabla} \times \vec{B} = \mu_0 \vec{J} + \mu_0 \epsilon_0 \frac{\partial \vec{E}}{\partial t} \tag{2.7.4}$$

where the charge density, ρ, and the current density, $\vec{J}$, are given by

$$\rho = ne \quad , \quad \vec{J} = ne\vec{u} \tag{2.7.5}$$

and ϵ_0 is the permittivity and μ_0 is the permeability of free space.

Applying the MHD equations to ionospheric plasma with the assumption of electrical neutrality to a compressible, collisionless plasma fluid in the absence of gravitational forces the appropriate equations governing its behavior are the continuity equation

$$\frac{\partial n}{\partial t} + \vec{\nabla} \cdot (n\vec{u}) = 0 \tag{2.7.6}$$

and the momentum equation

$$nm[\frac{\partial \vec{u}}{\partial t} + (\vec{u} \cdot \vec{\nabla})\vec{u}] + \vec{\nabla} p - ne(\vec{E} + \vec{u} \times \vec{B}) = 0 \tag{2.7.7}$$

where n is the plasma density, $\vec{u}$ is velocity, and p is pressure taken to be scalar.

For $p = nKT$, momentum equation becomes

$$nm[\frac{\partial \vec{u}}{\partial t} + (\vec{u} \cdot \vec{\nabla})\vec{u}] + KT\vec{\nabla}n - ne(\vec{E} + \vec{u} \times \vec{B}) = 0 \tag{2.7.8}$$

where K is Boltzmann constant and T is temperature.

By taking the curl of Eq. (2.7.2) gives

$$\vec{\nabla} \times (\vec{\nabla} \times \vec{E}) = -\frac{\partial}{\partial t}(\vec{\nabla} \times \vec{B}) \tag{2.7.9}$$

Substituting Eq. (2.7.4) into Eq. (2.7.9) and using the vector relation
$\vec{\nabla} \times (\vec{\nabla} \times \vec{E}) = \vec{\nabla}(\vec{\nabla} \cdot \vec{E}) - \nabla^2\vec{E}$ yields the following equation:

$$\nabla^2\vec{E} - \mu_0\epsilon_0\frac{\partial^2\vec{E}}{\partial^2 t} - \vec{\nabla}(\vec{\nabla} \cdot \vec{E}) = \mu_0\frac{\partial \vec{J}}{\partial t} \tag{2.7.10}$$

The equilibrium state of the plasma is established, the characteristic waves that can propagate in the plasma can be calculated by perturbing this equilibrium state. This is accomplished by perturbing the plasma parameters, the electric field and the magnetic fields, as follows:

$$\begin{aligned} n(\vec{r}, t) &= n_0 + n_1(\vec{r}, t) \\ \vec{u}(\vec{r}, t) &= \vec{u}_0 + \vec{u}_1(\vec{r}, t) \\ \vec{E}(\vec{r}, t) &= \vec{E}_0 + \vec{E}_1(\vec{r}, t) \\ \vec{B}(\vec{r}, t) &= \vec{B}_0 + \vec{B}_1(\vec{r}, t) \end{aligned} \tag{2.7.11}$$

where the subscript 1 is used to denote a small perturbation. Using these perturbation quantities and neglecting the nonlinear terms, taking account of the fact that the equilibrium parameters $(n_0, \vec{u}_0, \vec{E}_0, \vec{B}_0)$ are constant, Eqs. (2.7.6, 2.7.8, 2.7.10) become

$$\frac{\partial n_1}{\partial t} + n_0\vec{\nabla} \cdot \vec{u}_1 + \vec{u}_0 \cdot \vec{\nabla}n_1 = 0 \tag{2.7.12}$$

$$n_0m[\frac{\partial \vec{u}_1}{\partial t} + (\vec{u}_0 \cdot \vec{\nabla})\vec{u}_1] + KT\nabla n_1 - n_0e(\vec{E}_1 + \vec{u}_1 \times \vec{B}_0 + \vec{u}_0 \times \vec{B}_1) = 0 \tag{2.7.13}$$

$$\nabla^2\vec{E}_1 - \mu_0\epsilon_0\frac{\partial^2\vec{E}_1}{\partial^2 t} - \vec{\nabla}(\vec{\nabla} \cdot \vec{E}_1) = \mu_0\frac{\partial \vec{J}_1}{\partial t} \tag{2.7.14}$$

where $\vec{J}_1 = en_1\vec{u}_1$ is the perturbed current density.

For small perturbations, the perturbed quantities can be described by plane waves:

$$n_1, \vec{u}_1, \vec{E}_1, \vec{B}_1 \propto e^{i(\vec{k}\cdot\vec{r} - \omega t)} \tag{2.7.15}$$

Therefore, when $\vec{\nabla}$ and $\frac{\partial}{\partial t}$ operate on perturbed quantities, they can simply be replaced by

$$\vec{\nabla} \rightarrow i\vec{k} \ , \ \frac{\partial}{\partial t} \rightarrow -i\omega \tag{2.7.16}$$

In this case, the partial differential Eqs. (2.7.12-2.7.14)) reduce to the algebraic equations:

$$(\omega - \vec{k} \cdot \vec{u}_0)n_1 = n_0 \vec{k} \cdot \vec{u}_1 \tag{2.7.17}$$

$$i(\omega - \vec{k} \cdot \vec{u}_0)\vec{u}_1 - i\vec{k}\frac{KT}{n_0 m}n_1 + \frac{e}{m}(\vec{E}_1 + \vec{u}_1 \times \vec{B}_0 + \vec{u}_0 \times \vec{B}_1) = 0 \tag{2.7.18}$$

$$(\frac{\omega^2}{c^2} - k^2)\vec{E}_1 + \vec{k}(\vec{k} \cdot \vec{E}_1) = -i\omega\mu_0 \vec{J}_1 \tag{2.7.19}$$

For purely transverse waves $\vec{k} \cdot \vec{E}_1 = 0$, and, the general wave equation (Eq. (2.7.19)) reduces to

$$(\frac{\omega^2}{c^2} - k^2)\vec{E}_1 = -i\omega\mu_0 \vec{J}_1 \tag{2.7.20}$$

The perturbed current density is obtained by a linearization of the total current density, J, which for a two-component plasma is given by

$$\vec{J} = n_i e\vec{u}_i - n_e e\vec{u}_e \tag{2.7.21}$$

The linearization is accomplished by first perturbing the densities and drift velocities as follows

$$\begin{aligned} n_e &= n_{e0} + n_{e1} \\ n_i &= n_{i0} + n_{i1} \\ \vec{u}_e &= \vec{u}_{e0} + \vec{u}_{e1} \\ \vec{u}_i &= \vec{u}_{i0} + \vec{u}_{i1} \end{aligned} \tag{2.7.22}$$

Substituting Eq. (2.7.22) into Eq. (2.7.21) and neglecting the nonlinear terms yields the following expression for the current density:

$$\vec{J} = \vec{J}_0 + \vec{J}_1 \tag{2.7.23}$$

where

$$\vec{J}_0 = n_{e0} e(\vec{u}_{i0} - \vec{u}_{e0}) \tag{2.7.24}$$

$$\vec{J}_1 = n_{e0} e(\vec{u}_{i1} - \vec{u}_{e1}) + n_{i1} e\vec{u}_{i0} - n_{e1} e\vec{u}_{e0} \tag{2.7.25}$$

The current J_0 is the current that flows in the undisturbed plasma, and J_1 is the perturbed current associated with the electromagnetic wave. It is instructive to consider

first the propagation of electromagnetic waves in a plasma that is not subjected to either electric or magnetic fields ($\vec{E}_0 = \vec{B}_0 = 0$). For simplicity, the plasma is also assumed to be electrically neutral ($n_{e0} = n_{i0}$), stationary ($\vec{u}_{e0} = \vec{u}_{i0} = 0$), cold ($T_e = T_i = 0$), uniform, and steady. When an electromagnetic wave propagates through such a plasma, a current is induced and the disturbed plasma then affects the electromagnetic wave. The fact that the waves are high frequency means that the ions do not participate in the wave motion. Physically, the ion inertia is too large and the ions can not respond to the rapidly fluctuating waves. Therefore, the ion equations of motion can be ignored, and the ions merely provide a stationary background of positive charge. With these simplifying assumptions, the perturbed current density (Eq. (2.7.25)) and the electron momentum (Eq. (2.7.18)) reduce to

$$\vec{J}_1 = -n_{e0} e \vec{u}_{e1} \tag{2.7.26}$$

$$i\omega \vec{u}_{e1} - \frac{e}{m_e}\vec{E}_1 = 0 \tag{2.7.27}$$

Substituting $\vec{u}_{e1}$ from Eq. (2.7.27) into Eq. (2.7.26) and then substituting that result into Eq. (2.7.20), which gives

$$\vec{E}_1(\frac{\omega^2}{c^2} - k^2 - \mu_0 \epsilon_0 \omega_{pe}^2) = 0 \tag{2.7.28}$$

The fluctuating electric field is not zero and, therefore, the quantity in the brackets must be zero, which yields

$$\omega^2 = \omega_{pe}^2 + c^2 k^2 \tag{2.7.29}$$

Eq. (2.7.29) is a dispersion relation for transverse electromagnetic waves of angular frequency ω in an electron plasma frequency $\omega_{pe}^2 = \frac{n_{e0}e^2}{\epsilon_0 m_e}$.

The wave number $\vec{k}$ can be written as $\vec{k} = \frac{n\omega}{c}$, where n is the index of refraction. From Eq. (2.7.29) the phase index of refraction of a plasma is then given by

$$n_{ph}^2 = 1 - \frac{\omega_{pe}^2}{\omega^2} \tag{2.7.30}$$

Eq. (2.7.30) is the Appleton-Hartree equation describing the dispersion encountered by an electromagnetic wave upon transmision through plasma. Since the ionosphere is a partially ionized plasma, Eq. (2.7.30) is the basic equation in understanding satellite signal transmission through the ionosphere. For high frequency radiation($\omega > \omega_{pe}$) the index of refraction is real and less than 1, thus the wave travel in the ionosphere faster than vacuum i.e. the phase is advanced.

The group refractive index, n_g, is given by

$$n_g = \frac{c}{u_g} = c\frac{dk}{dw} = \frac{d(wn_{ph})}{dw} \tag{2.7.31}$$

The general relationship between the group refractive index, n_g, and the phase refractive index, n_{ph}, for a non-isotropic medium, is given by

$$n_g = n_{ph} + w\frac{dn_{ph}}{dw} \tag{2.7.32}$$

Substituting Eq. (2.7.30) in Eq. (2.7.32) and with the requirement $\omega > \omega_{pe}$ the group refractive index becomes

$$n_g^2 = \frac{1}{1 - \frac{\omega_{pe}^2}{\omega^2}} \tag{2.7.33}$$

The fact that n_g is greater than 1 in Eq. (2.7.33) for high frequency radiation ($\omega > \omega_{pe}$) means the wave group travels slower in the ionosphere than its speed in vacuum i.e. the wave group is delayed.

For frequencies lower than the electron plasma frequency ω_{pe} , n_{ph} is imaginary, consequently such electromagnetic waves incident on ionosphere will be reflected from the surface.

Chapter 3

Vertical Ionospheric Sounding

3.1 Introduction

Both vertical and oblique ionospheric sounders operate on the same principles. However the geometry of the vertical case is more straightforward to interpret and have been used in this thesis to compare with the model measurements. Vertical ionosondes are radars that transmit HF radio waves vertically up to the ionosphere. Receive antennas installed with the transmitter detect the return echoes from the ionosphere . The time of flight of the radio signals at a particular frequency gives an indication of the height of the reflecting layer.

3.2 The ionosonde

Ionosonde, one of the first radar sounding techniques, provides direct and accurate measurements of the ionospheric plasma density. It is a high frequency radar which sends very short pulses of radio energy vertically into the ionosphere. If the radio frequency is not too high, the pulses are reflected back towards the ground. During reflection electron density values are calculated from reflected radio waves corresponding to the density dependent critical frequency of the ionized plasma and density heights are inferred from the time delay of the reflected radio waves. The ionosonde provides estimates of electron density maxima of each layer and the estimated altitude at which the density occurred, as a function of time.

The ionosonde consists of transmitter and receiver with coupled tuning circuits, which is a sweep in frequency usually in a frequency range of 0.1 to 30 MHz [12]. After the RF signals have been reflected by the ionosphere they are received and processed by the receiver to produce ionograms. All transmitted frequencies above the critical frequency will penetrate the layer without being reflected. Their group velocity will however, will be slowed by any ionisation, and this will add to the time of flight. If such a wave encounters another layer, whose plasma frequency is higher than the frequency of the wave, it will be reflected, and the return signal will be further delayed as it travels back through the underlying ionisation. The apparent, or virtual height indicated by this time delay will therefore be greater than the true height. The difference between true height and virtual height is governed by the amount of ionisation that the wave has passed through [13].

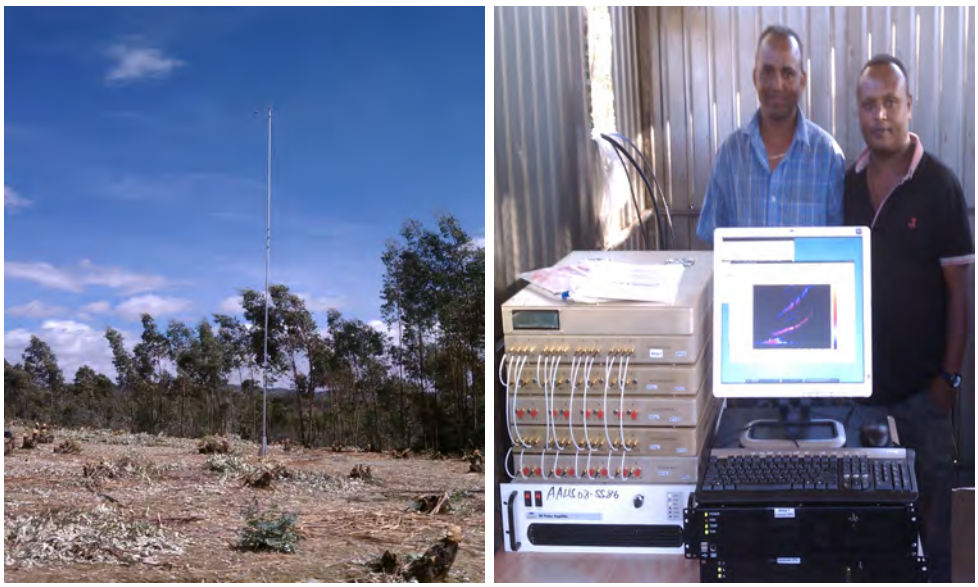

(a) (b)

Figure 3.1: (a) The transmitter and receiver antenna and (b) data analysis system of the welmera station ionosonde.

The pulse ionosonde transmits short pulses of radio energy and records the time delay of the reflection of the echo by the ionosphere. The virtual height of reflection (h') is the apparent height of an ionized layer had the wave continued to travel at the speed of light, as determined from the time interval between the transmitted signal and the ionospheric echo at vertical incidence. It is given by

$$h' = \frac{1}{2} c \Delta t \tag{3.2.1}$$

where c is the speed of light, Δt is the time delay and the factor 2 accounts for the fact that the pulse has to traverse the distance h' twice. However the true altitude of the reflecting layer has to allow for the true speed at which the radio wave has travelled:

$$h' = c \int_0^{h_r} \frac{dh}{u_g} \tag{3.2.2}$$

where u_g is the group velocity and h_r is the real height of reflection [11].
In terms of group refractive index Eq. (3.2.2) for the virtual height measured by an ionosonde becomes

$$h' = \int_0^{h_r} n_g dh \tag{3.2.3}$$

Substituting Eq. (2.7.33) in Eq. (3.2.3) provides

$$h' = \int_0^{h_r} \frac{1}{\sqrt{(1 - \frac{\omega_{pe}^2}{\omega^2})}} dh \tag{3.2.4}$$

Using $\omega_{pe}^2 = \frac{Ne^2}{\epsilon_0 m_e}$, Eq. (3.2.4) becomes

$$h' = \int_0^{h_r} \frac{1}{\sqrt{(1 - \frac{N(h)e^2}{\epsilon_0 m_e \omega^2})}} dh \tag{3.2.5}$$

The virtual height, h', or equally the time of flight of the radio pulse, is what is measured and N(h) is what is required in order to analyse how a radio signal would propagate through an ionosphere for communications purposes.

Limitation of all ionosondes is that they can give information on the ionosphere only up to the height of maximum ionization of the F2 layer, unless one extends end of the sweep by an increasing the height of the transmitting antenna tower and using relatively higher power not much information can be obtained from the D region. Because low frequency radio waves are absorbed by the D region. During sudden ionospheric disturbances (SIDs) and intense polar cap precipitation of solar energetic particles, D region ionization can become so intense that HF radio communication is completely blacked out. In this case information from ionosonde is limited. The path of radio wave is affected by any free charges in the medium through which it is travelling. The refractive index (the ratio of the phase velocity in free space to the phase velocity in the medium) is governed by the electron concentration and the magnetic field of the medium as well as the frequency and polarisation of the transmitted wave.

3.3 The ionogram

When the pulses of high frequency are broadcast by an ionosonde they are reflected by the ionosphere and return to the receiver. The time necessary for the occurrence of this feature is stored in the form of traits called ionograms. It is a graph of time of flight against transmitted frequency. The ionograms generated by ionosondes are analyzed and interpreted to obtain the ionospheric parameters, such as the plasma frequency of the ionospheric layers, reflection or critical frequencies of the layers E, F1 and F2, i.e. foE, foF1, foF2, their minimum virtual heights of reflection h'E, h'F1 and h'F2, and the vertical profile of electron density from the bottom of the ionosphere up to the peak of maximum density. The critical frequency of each layer is scaled from the asymptote and the virtual height of each layer is scaled from the lowest point on each curve [13].

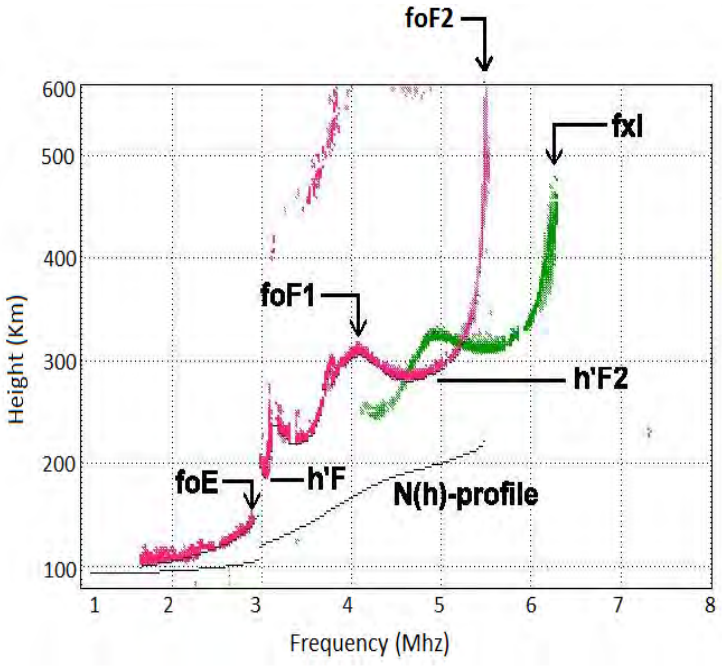

Figure 3.2: Empirical Illustration of the idealized ionogram (from [14]).

This figure shows echoes from the E region, the F1 region, and the F2 region. Following the trace from its beginning around 1.6 MHz, we see that the virtual height steadily increases as frequency increases. Just before 3 MHz the trace rises steeply, this is the E region critical frequency (annotated as foE), indicating that the E region electron density at this frequency is not dense enough to turn the pulse back to Earth. Similarly, another

steep rise in virtual height is seen around 5.5 MHz, this is the F2 region critical frequency (annotated foF2). Note the slight hump in the trace around 4.2 MHz that's annotated foF1, this is the F1 critical frequency. There is no steep rise in virtual height as seen with foE and foF2 because the F1 region does not have an electron density peak as do the E and F2 regions. The F1 region is more of an inflection point in the electron density.

The presence of the Earth's magnetic field makes the ionosphere a doubly refracting medium for radio wave propagation. This explains the two traces on the ionogram. The red and green traces represent the ordinary (O) wave and the extraordinary (X) wave respectively (see Fig. 3.3). This is a result of the magnetic field, which causes the ionosphere to be bi-refractive (or double refraction, is the decomposition of a radio wave into two rays when it passes through the ionospheric medium) [7].

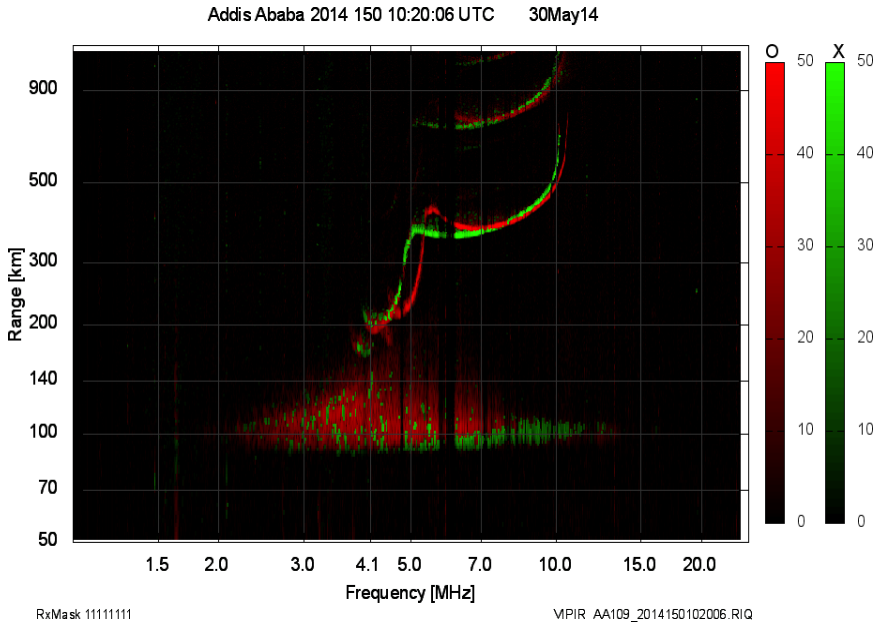

Figure 3.3: Ionogram recorded at Welmera station for the day 30/5/2014 at 10:20UT.

The red trace, or ordinary wave, in the ionogram is the returned echoes from the component of the transmitted radio signal that is parallel with the direction of the Earth's magnetic field. The green trace is the extraordinary wave, which is the component of the incident radio wave perpendicular to the magnetic field direction.

3.4 The interpretation of the ionograms

The ionosphere is a doubly refracting medium for the propagation of radio waves, being a plasma in the earth's magnetic field. Propagation is described by the Appleton-Hartree equation, which can be written as follows [12]:

$$n^2 = 1 - \frac{X}{(1 - iZ) - [\frac{Y_T^2}{2(1-X-iZ)}] \pm \sqrt{\frac{Y_T^4}{4(1-X-iZ)^2} + Y_L^2}} \tag{3.4.1}$$

where $X = \frac{\omega_{pe}^2}{\omega^2}$, $Y = \frac{\omega_{ce}}{\omega}$, $Z = \frac{\nu}{\omega}$, $Y_T = Y sin\theta$ and $Y_L = Y cos\theta$.
If we ignore the collision term, Eq. (3.4.1) can be written as

$$\mu^2 = 1 - \frac{X(1-X)}{(1-X) - \frac{1}{2}Y_T^2 \pm \sqrt{\frac{1}{4}Y_T^4 + (1-X)^2 Y_L^2}} \tag{3.4.2}$$

The reflection condition $\mu = 0$ gives two solutions for X;

A wave vertically incident on the ionosphere is reflected at a level where $\mu^2 = 0$. Thus for O wave

$$X = 1$$

so that

$$\omega_0 = \omega_{pe} \tag{3.4.3}$$

which means that for the O-wave, the plasma frequency for reflection is equal to the sounding frequency.

for the X-wave, it is found that reflection occurs at a level where $\mu^2 = 0$ and for perpendicular reflection

$$X = \begin{cases} 1 - Y & \text{when } Y < 1, \omega > \omega_{ce} \\ 1 + Y & \text{when } Y > 1, \omega < \omega_{ce} \end{cases} \tag{3.4.4}$$

For $Y < 1$ we have for reflection $X = 1 - Y$

$$\frac{\omega_{pe}^2}{\omega_x^2} = 1 - \frac{\omega_{ce}}{\omega} \tag{3.4.5}$$

which leads to

$$\omega_{pe}^2 = \omega_x^2 - \omega_x \omega_{ce} \tag{3.4.6}$$

Thus, for $Y < 1$, the plasma frequency for reflection of the X-wave is less than the sounding frequency.

Charged particles, electrons, cannot move across a magnetic field line but are forced to spiral around the line. The rate at which they rotate is called the gyrofrequency, which varies with position on the globe.

It is of interest to determine the separation in frequency of two waves of opposite mode reflected from the level of maximum electron density at the peak of a layer. Since the plasma density at the peak is the same for both waves, the plasma frequency will be the same so we can eliminate ω_{pe} from Eq. (3.4.3) and Eq. (3.4.6) to give

$$\omega_{0m}^2 = \omega_{xm}^2 - \omega_{xm}\omega_{ce} \tag{3.4.7}$$

Dividing Eq. (3.4.7) by $4\Pi^2$ gives

$$f_{0m}^2 = f_{xm}^2 - f_{xm}f_{ce} \tag{3.4.8}$$

thus

$$f_{ce} = \frac{f_{xm}^2 - f_{0m}^2}{f_{xm}} \tag{3.4.9}$$

and

$$f_{xm} = \frac{f_{ce} \pm (f_{ce}^2 + 4f_{0m}^2)^{\frac{1}{2}}}{2} \tag{3.4.10}$$

For $f_{om} >> f_{ce}$, ignoring the - sign,

$$f_{xm} = \frac{f_{ce} + 2f_{0m}}{2} = f_{0m} + \frac{f_{ce}}{2} \tag{3.4.11}$$

This formula is very useful in ionogram interpretation for deducing the critical frequency of penetration of a particular layer for the O-wave from the X-wave when the former is not visible for some reason, and vice versa.

Chapter 4

Semi Emperical Model

4.1 Introduction

To make adequate use of the ionosphere as a natural resource for radio propagation, both in terms of the application of radio propagation and for commercial and hobby radio enthusiasts, accurate measurements of ionospheric behaviour are required. When measurements are not available, it is necessary to develop an ionospheric model for a wide variety of uses. One of this model is the quick-run ionospheric electron (NeQuick) model. It is an empirical model of the ionosphere primarily intended for computing the TEC along the ray from a navigation satellite to a receiving site. It uses global ionosonde network data and allows for indices of solar activity. NeQuick provides vertical profiles of the electron density up to a height of 1000 km as functions of time and coordinates.

4.2 NeQuick model

NeQuick is an empirical quick-run ionospheric model, suitable for trans-ionospheric applications, which generates electron density for a given space, time and solar activity conditions from a minimum set of anchor points characteristics. It consists of two major components: the bottom side based on a modified version of the DGR model which contains ITU- R coefficients for foF2 and M(3000)F2 and simplified models for foF1 and foE that take into account the solar zenith angle, season and solar activity, and the topside model for the height region above the F2-layer peak, represented by a semi-Epstein layer with a height dependent thickness parameter.

NeQuick FORTRAN 77 code was accepted by the International Telecommunication Union Radiocommunication Sector (ITU-R) in 2000 and revised in 2002. It is referred to either as version 1 or ITU-R [15]. The input arguments are position with height h, geographic latitude Φ and longitude θ, season with month, solar activity with monthly smoothed value of the solar radio flux at a wavelength of 10.7cm (Φ12 or F10.7) and time of day with universal time UT. The basic parameters are then computed from these inputs and from CCIR maps [16].

In NeQuick, geomagnetic latitude is computed from the International Geomagnetic Reference Field (IGRF) model for the Earth's magnetic field [17] as a 3rd order Lagrange interpolation on a grid of data stored in the file diplats.asc. As a matter of fact, strictly speaking, the coordinates derived from such a model are defined as Corrected Geomagnetic Coordinates (CGM) [18], compared to typical geomagnetic coordinates derived from a dipole approximation. When NeQuick calculates magnetic dip and MODIP using CGM coordinates instead of using geomagnetic coordinates, these parameters should be denominated as Corrected Magnetic Dip (I) and Corrected Modified Dip Latitude (MODIP) respectively.

Chapter 5

Data and Methodologies

5.1 Data

The NeQuick model has been adopted for assessment studies by the European Space Agency European Geostationary Navigation Overlay Service (EGNOS) project and more recently by ITU-R as a suitable method for computing ionospheric electron density profile and TEC modeling. It was written in FORTRAN 77 by Dr. Reinhart Leitinger. The standard NeQuick source code is available at http://www.itu.int/ITU-R/study- groups/software/rsg3-p531-electron-density.zip.

The second data we used for this thesis is the ionosonde data, which is obtained from the newly installed HF-viper radar found at Welmera site. The data consists of height of reflection of waves and frequency reflected at the given height. Then the electron density is calculated from the frequency-electron density relating equation.

5.2 Key parameters

The NeQuick model is a user-friendly quick-run model for trans-ionospheric applications that enables the calculation of either the vertical or slant electron density profile and the total electron content (TEC) for any specified path.

NeQuick is a three dimensional and time dependent ionospheric electron density model developed at the Aeronomy and radiopropagation laboratory at the Abdus Salam International Center for theoretical physics (ICTP), Trieste, Italy and the Institute for Geophysics, Astrophysics and Meteorology of the University of Graz, Austria [19].

It is a profiler which uses the peaks of the E-layer, F1-layer and F2-layer as anchor points related to the ionospheric characteristics routinely scaled from ionograms.

To model the anchor points it uses the "ionosonde parameters" foE, foF1, foF2 (critical frequencies) and M(3000)F2 (transfer parameter). For foE it uses a model by John Titheridge; foF1 is taken to be proportional to foE during daytime ($foF1 = 1.4 \times foE$) and zero during nighttime. For foF2 and M(3000)F2 it uses the ITU-R (CCIR) coefficients.

The NeQuick model input are the position, the epoch and the solar activity and as output, the model provides the ionospheric and plasmaspheric electron density as a function of height, latitude and longitude, solar activity, month, and universal time. The electron concentration can be calculated along an arbitrarily chosen ray path and the resultant profile is smooth (continuous first-order spatial derivatives) which is important for ray tracing and location finding applications.

The electron density at any location is computed based on the characteristic parameters of the anchor points at a given location and time of the ionosphere. The formulation of the NeQuick model is based on the Epstein layer so we need to explain the Epstein layer. The Epstein layer is an electron density function built on Epstein function and represented by the following expression [20, 21, 22]:

$$N(h) = \frac{4N_{max}}{(1 + exp(\frac{h-h_{max}}{B}))^2} exp(\frac{h - h_{max}}{B}) \tag{5.2.1}$$

where $N(h)$ is the electron at height h, N_{max} is the peak electron density, h_{max} the height of the peak electron density and B is the thickness of the layer.

The electron density of the Epstein layer is a symmetric function and has a parabolic form around the height of the electron density. Better results from NeQuick model are obtained by considering different values of the thickness of the bottom and top parts of the Epstein layer associated to each ionospheric region (E, F1, F2) [23, 24]. Based on this, the formulation of NeQuick for the bottom side ($h \leq h_{max}, F2$) is based on the five semi-Epstein layers. These are two semi-Epstein layers from E region (top and bottom), two for the F1 region(top and bottom) and for the bottom of F2 region. But NeQuick does not take any characteristic parameters of the D region in to account [25]. The electron density at any given height less than the height of peak electron density of the bottom

side of F2 region is computed by summation of the three semi-Epstein layers[26]. Thus

$$N(h) = \sum_{E,F1,F2} N_i(h) \tag{5.2.2}$$

where

$$N_i(h) = \frac{4A_i}{(1 + exp(Z_i))^2} exp(Z_i)$$

A radio wave propagating into the ionospheric plasma encounters a medium with the refractive index n (in the absence of the earth's magnetic field and ignoring collisions between electrons and the neutral atmosphere)

$$n^2 = 1 - X = 1 - \frac{f_N^2}{f^2} \tag{5.2.3}$$

where

$$X = \frac{N_e e^2}{4\pi^2 \epsilon_0 m f^2}$$

and e, ϵ_0, m are natural constants, N_e is the electron density and f is the wave frequency. Below the ionosphere, $N_e = 0$, and $n = 1$. Within the ionosphere, $N_e > 0$, and $n < 1$. At a level where $X = 1$,

$$f_N^2 = \frac{N_e e^2}{4\pi^2 \epsilon_0 m} = f^2 \tag{5.2.4}$$

The refractive index n becomes zero. The wave cannot propagate any further and is reflected. The quantity f_N, which relates the electron density to the frequency being reflected, is called the plasma frequency. Inserting the natural constants into Eq. (5.2.4) permits us to deduce the useful relation between electron density and plasma frequency (which is identical to the probing frequency being reflected)

$$N_{ex} = 1.24 \times 10^4 (f_x)^2 \tag{5.2.5}$$

where x stands for E, F1 or F2 and f is in MHz and N_e in $electrons/m^3$.

5.3 Statistical Measures

The differences between the simulated and observed values (bias) are presented in percentages in order to make comparison easier. This is calculated as follows

$$Bias(\%) = \frac{1}{N}\sum_{i=1}^{N}(\frac{R^m - R^s}{R^m})100\% \tag{5.3.1}$$

where N is the number of data points, R^m is measured value and R^s is simulated value.

Root Mean Square Deviation (RMSD) is a frequently used measure of the differences between values simulated by a model and the the values actually observed. To statistically compare the performance of the simulated with respect to obsevations, the root mean square deviation (RMSD) values were calculated as follows [27]:

$$RMSD = \sqrt{\frac{1}{N}\sum_{i=1}^{N}(R^m - R^s)^2} \tag{5.3.2}$$

where N is the number of data points, and R^m and R^s are measured and simulated values respectively.

Correlation coefficient is a statistical measure of the degree to which changes to the value of one variable predict change to the value of another.Correlation coefficients are expressed as values between +1 and -1. A coefficient of +1 indicates a perfect positive correlation and a coefficient of -1 indicates a perfect negative correlation. It can be defined as

$$R = \frac{1}{\delta_m \delta_s}(\sum_{i=1}^{N}(R^m - \bar{R}^m)(R^s - \bar{R}^s)) \tag{5.3.3}$$

where δ_m and δ_s are the standard deviations for measured (R^m) and simulated (R^s) values respectively and $\bar{R}^m$, $\bar{R}^s$ are their respective mean values.

Chapter 6

Results and Discussion

6.1 Ionospheric electron density from NeQuick and Ionosonde

Electron density profiles have been simulated using the NeQuick model over suitable grids of input parameters such as month, local time, geomagnetic latitude, solar activity, and in the altitude range between 100 km and 1000 km.

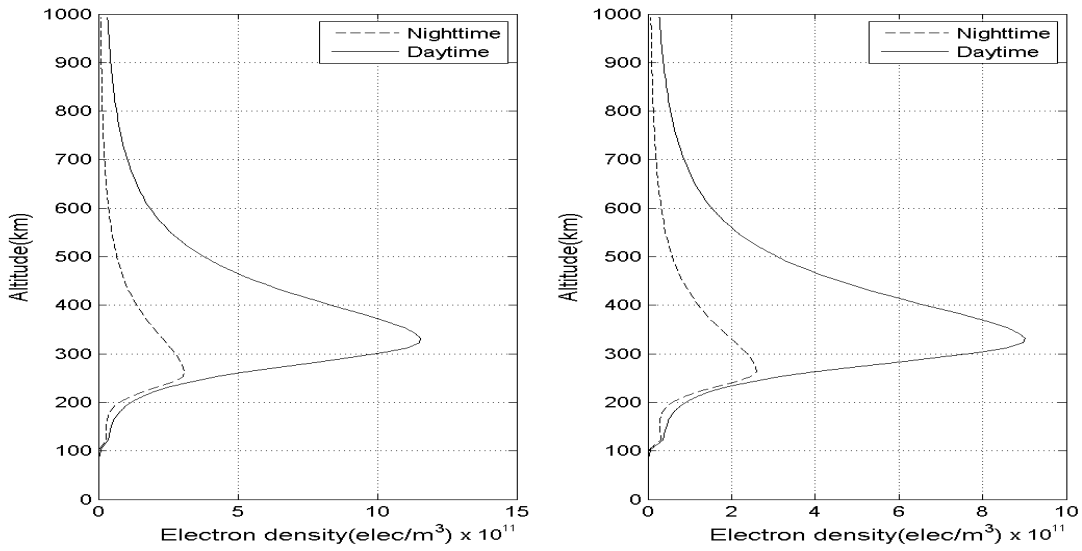

Figure 6.1: Electron density vertical distribution for day time at 13:10 UT (solid line) and for night time at 02:35 UT (dashed line) on May, 2014 (left panel) and on June, 2014 (right panel).

Fig. 6.1 (right panel) shows the peak electron density at day time (13:10UT) with a maximum of $11.5 \times 10^{11} electrons/m^3$ on may, 2014, where as on the same day during the night time the peak electron density (02:35UT) is $2.6 \times 10^{11} electrons/m^3$. On June 2014 (Fig. 6.1 left panel) the day time peak electron density is $9 \times 10^{11} electrons/m^3$ and night time electron density peak is $2.5 \times 10^{11} electrons/m^3$. This shows that the maximum peak electron density is obtained at day time and the minimum peak electron density is obtained at night time as expected from the theoretical formulation given in Chapter 2.

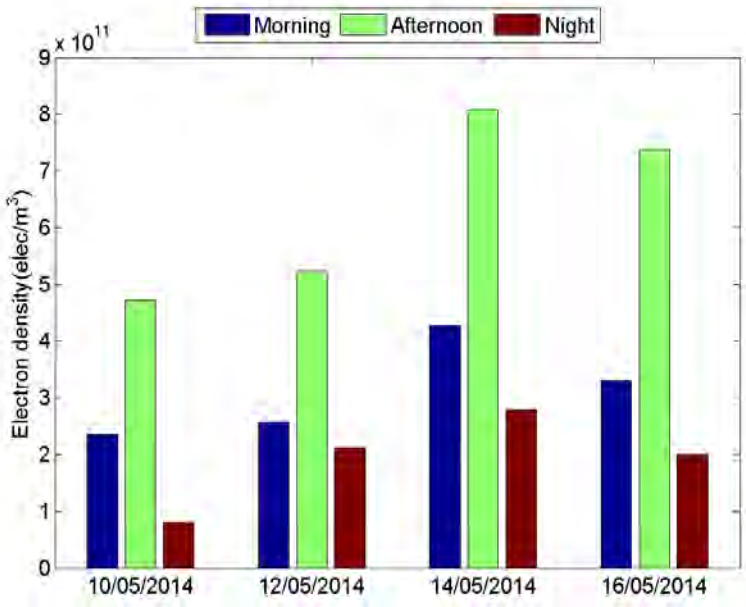

Figure 6.2: A bar graph of peak electron density from ionosonde measurements during the morning,afternoon and night time on different days in May, 2014.

Fig. 6.2 shows diurnal variation of electron density on a different date from ionosonde observation. Noon time peak electron density and night time minima are common feature of electron density on different dates. However, there is day to day differences on the magnitude of electron density observed at all times namely morning, noon and night.

6.2 Comparision of electron density from ionosonde and NeQuick model

For ionosonde and NeQuick model the electron density values were computed for January 2012, May, June and July 2014. The predicted electron density from NeQuick model is then compared with that from ionosonde. However, the topside ionospheric electron density can not be measured by ionosonde. So only the E, F1 and F2 regions are compared depending on the data availability.

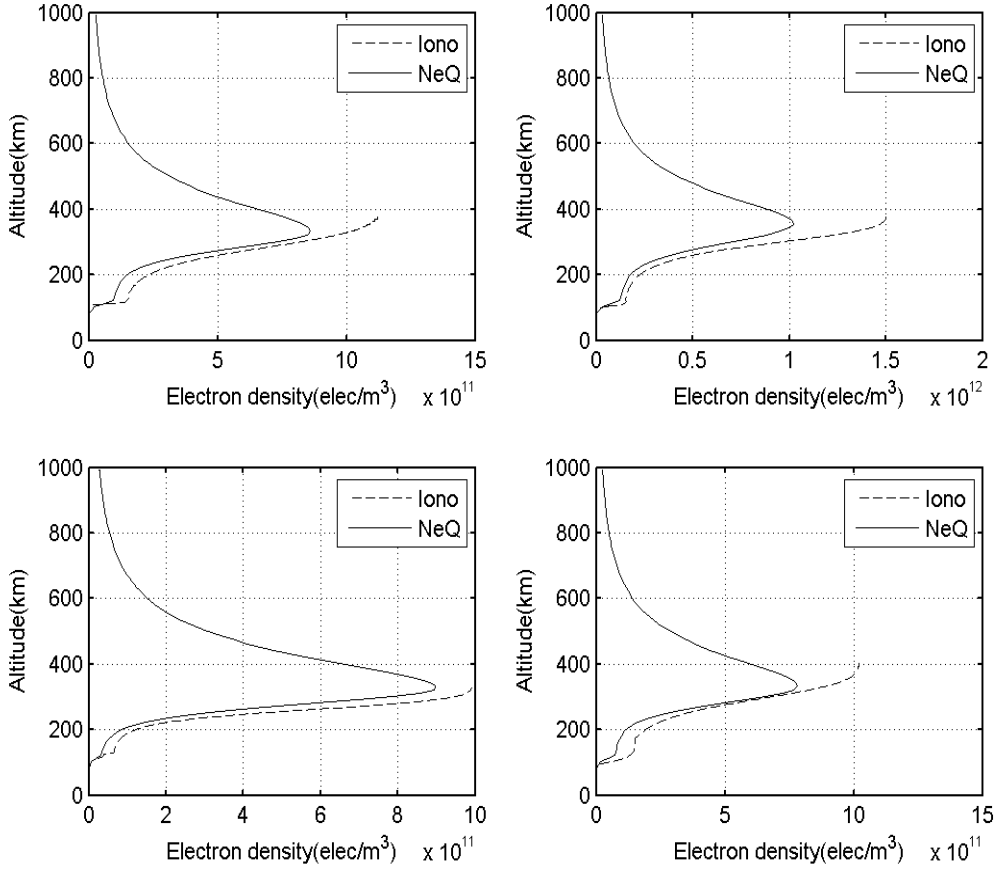

Figure 6.3: Comparison between the electron density profiles from the NeQuick model (NeQ) and from the ionosonde data (Iono) on January, 2012 at 13:30UT (top left), May, 2014 at 12:25UT (top right), June, 2014 at 15:45UT (bottom left) and July, 2014 (bottom right).

Fig. 6.3 shows the comparisons between the electron density profiles from the NeQuick model (annotated NeQ) and from ionosonde obsevation (annotated Iono). The agreement is generally good for all cases shown here except near peak electron density and below 200km altitude. NeQuick fails to capture peak electron density measured by ionosonde. This suggests that the model can only capture the general shape of the electron profile while day to day variation is difficult to capture since such variability is not part of the seasonal climatology incorporated in the model. Therefore, it is rather crucial to have in-situ observations up on which the model can be further tuned so that it capture the variability of electron density over this region.

To highlight the importance of such effort, we have extracted key parameters from ionosonde and used them in NeQuick instead of the climatological key parameters. The results are given in Section 6.3.

6.3 Comparision of electron density from ionosonde and NeQuick before and after ingestion of ionosonde key parameters

NeQuick was used to obtain electron density profile before and after ingesting the ionosonde key parameters (foE, hmE, foF2 and hmF2) recorded by the means of Ionosonde found at Welmere station. Both the NeQuick before (NeQ1) and NeQuick after (NeQ2) ingested computed electron density for selected time are compared to the electron density from the ionosonde measurements (Iono) are shown in Fig. 6.4 for January, 2012 and Fig. 6.5 for May, 2014 at different times respectively.

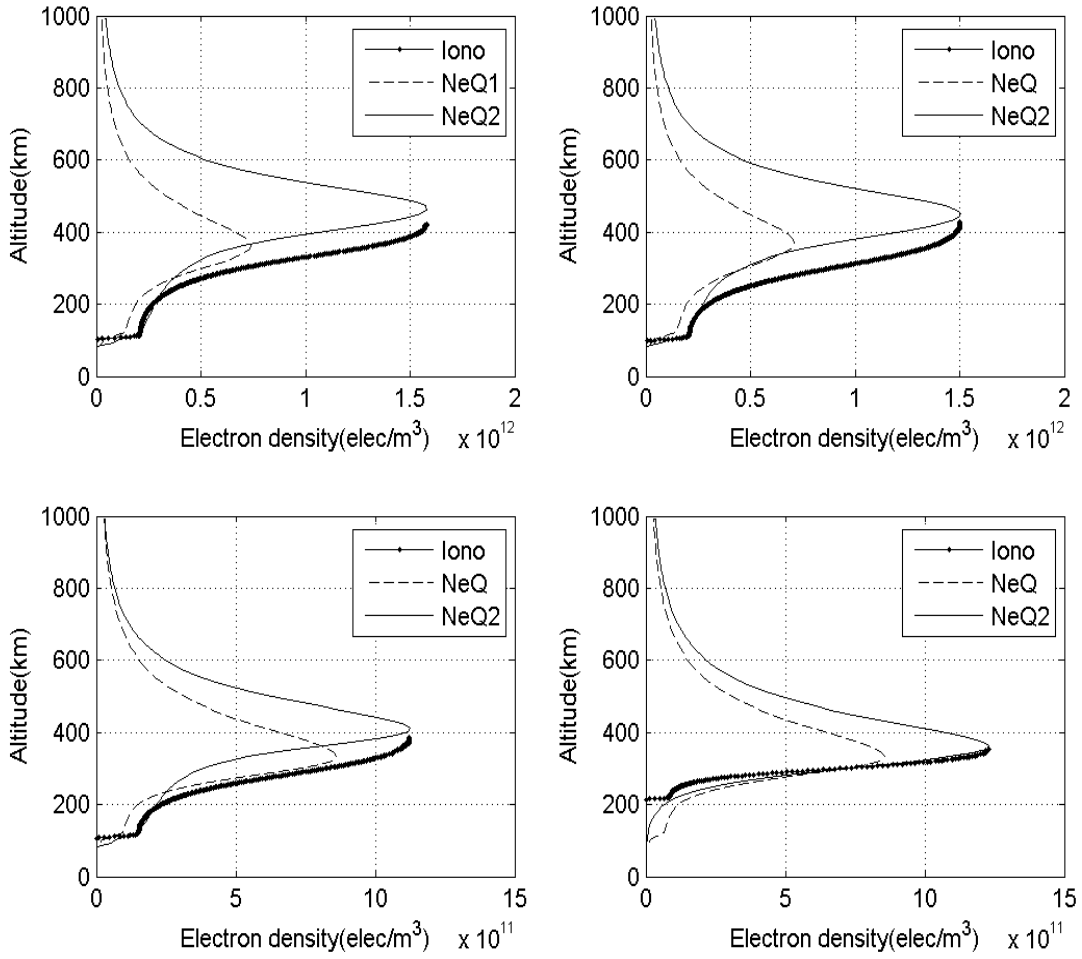

Figure 6.4: Evaluation of the NeQuick before (NeQ1) and after (NeQ2) ingestion of foE, hmE, foF2 and hmF2 with Ionosonde (Iono) on January, 2012 at 08:45UT (top-left), 09:05UT (top-right), 13:30UT (bottom-left) and 14:30UT (bottom-right) respectively.

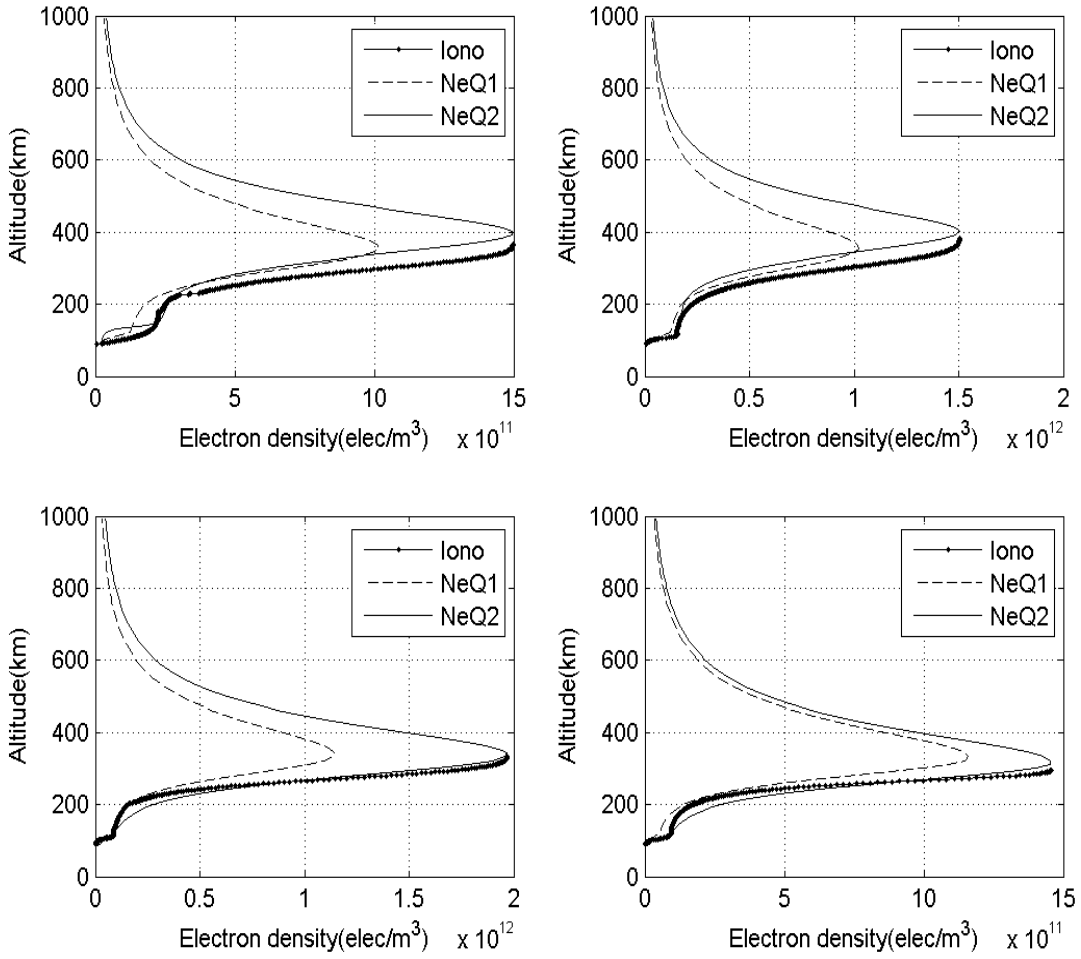

Figure 6.5: Evaluation of the NeQuick before (NeQ1) and after (NeQ2) ingestion of foE, hmE, foF2 and hmF2 with Ionosonde (Iono) on May, 2014 at 12:20UT (top-left), 12:25UT (top-right) , 14:40UT (bottom-left) and 15:00UT (bottom-right) respectively.

Figs. 6.6-6.7 also show similar comparison for ionosonde obsevations in June and July, 2014. The use of ionosonde key parameters namely foE, foF2, hmE and hmF2 in NeQuick model has improved the agreement between NeQuick model and ionosonde bottomside electron density profiles. The agreement between the model and ionosonde electron density as a result of use of the key parameter is much better in May-July, 2014 than January, 2012 period. The defference between the two periods is likely linked with presence moderate geomagnetic storm in January, 2012. This suggests that the need for more key parameters from ionosonde data than the current four parameters during storm time [28].

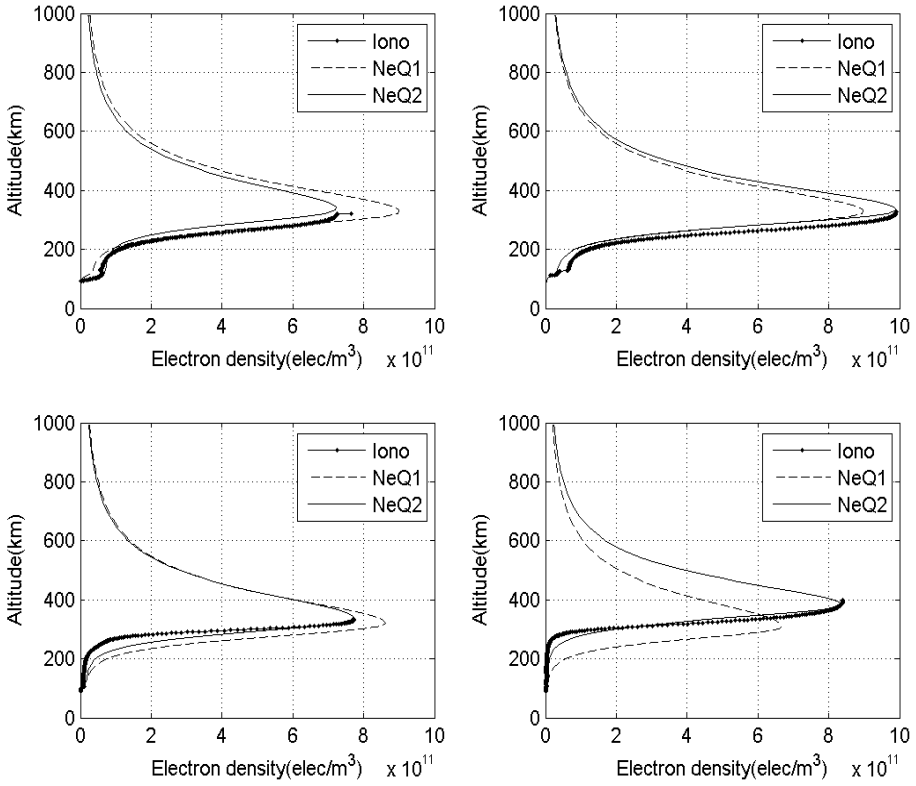

Figure 6.6: Evaluation of the NeQuick before (NeQ1) and after (NeQ2) ingestion of foE, hmE, foF2 and hmF2 with Ionosonde (Iono) on June, 2014 at 15:40UT (top-left), 15:45UT (top-right), 16:00UT (bottom-left) and 17:35UT (bottom-right) respectively.

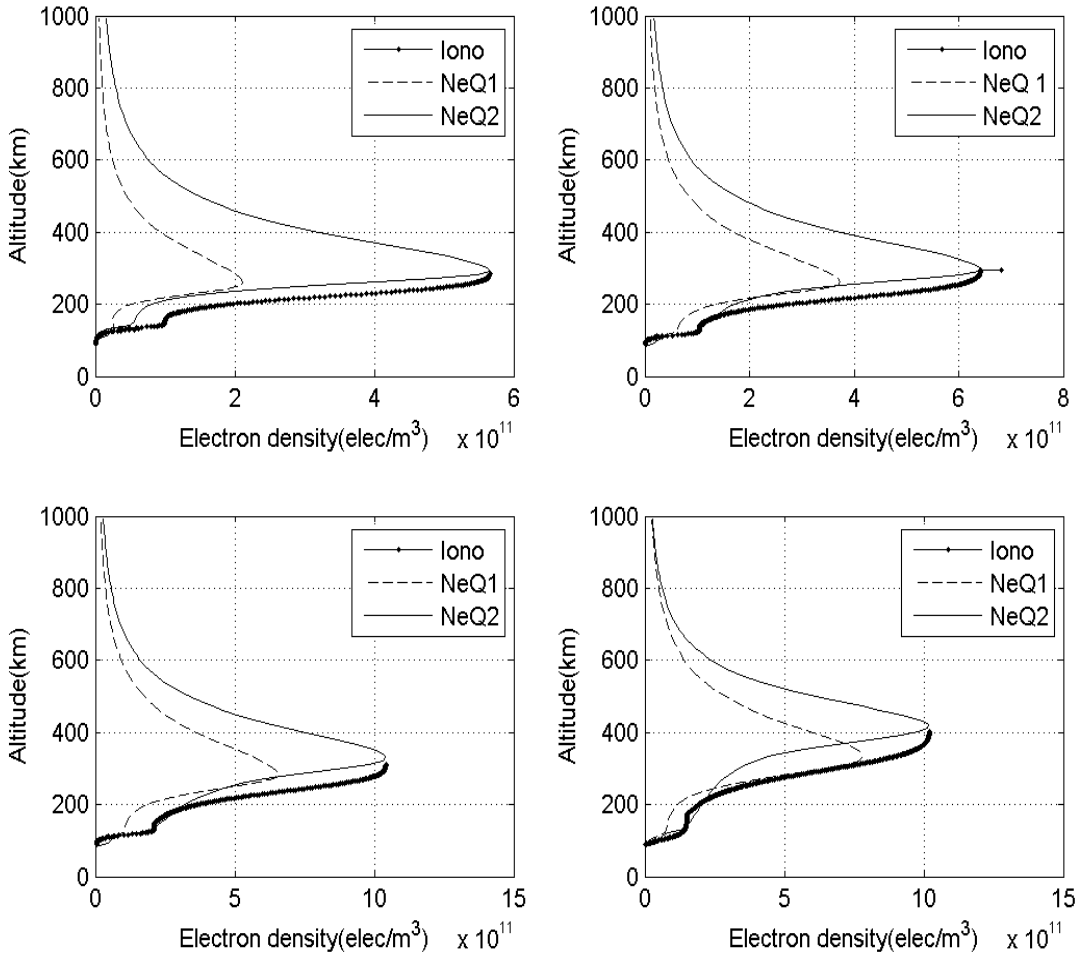

Figure 6.7: Evaluation of the NeQuick before (NeQ1) and after (NeQ2) ingestion of foE, hmE, foF2 and hmF2 with Ionosonde (Iono) on July, 2014 at 03:30UT (top-left), 23:00UT (top-right), 15:30UT (bottom-left) and 14:45UT (bottom-right) respectively.

Figs. 6.8-6.11 (left panels) show only bottom side ionosphere for the two simulations and ionosonde observations. The right panels show difference of the two simulations from ionosonde observations in January, 2012 and May, June, July, 2014 in percent of ionosonde electron density. The use of key parameters from ionosonde has reduced in the bias in simulated electron density from a maximum of 60% to 40% at some altitudes in January, 2012 (see Fig. 6.8)

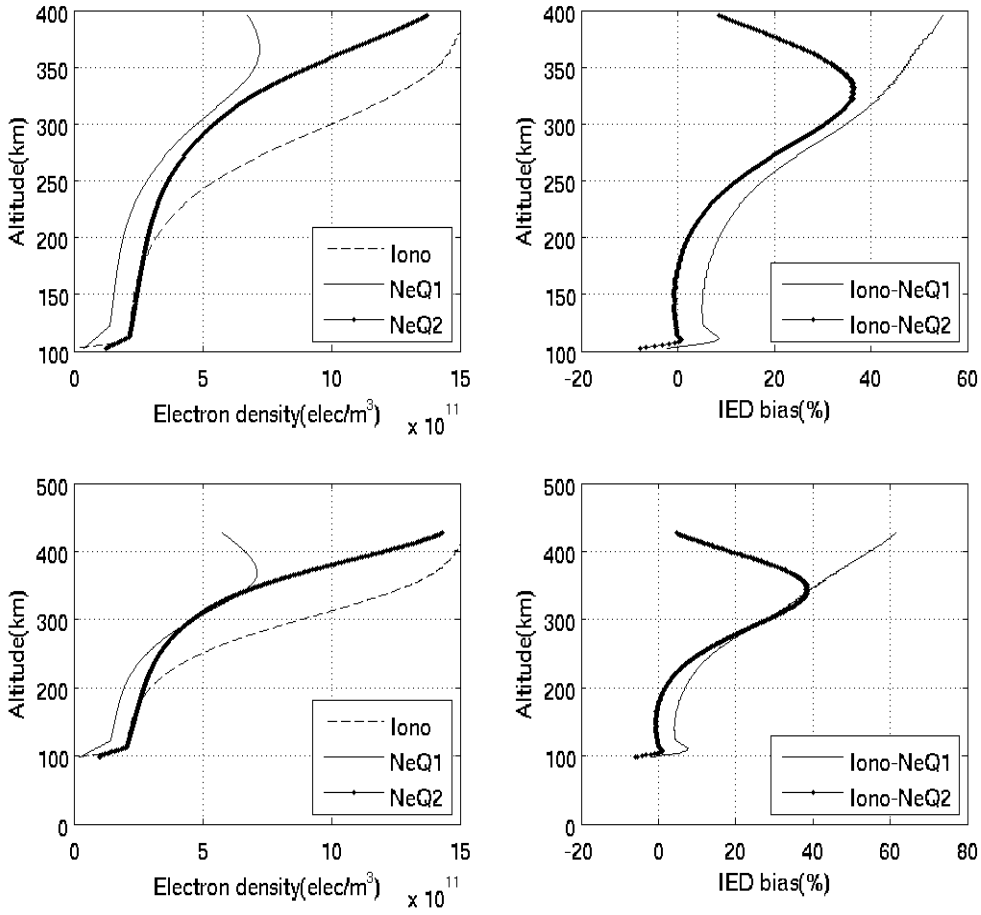

Figure 6.8: A bottomside electron density vertical distribution on January, 2012 at 08:45UT (top two panel) and at 09:05UT (bottom two panel).

Fig. 6.9 (left panels) show bottom side electron density from the two simulations and ionosonde for May, 2014. The left panels corresponding departure of the simulations from ionosonde. The improved simulation exhibits low bias of about 10% or less as compared to a maximum of 45% bias without key parameters from ionosonde.

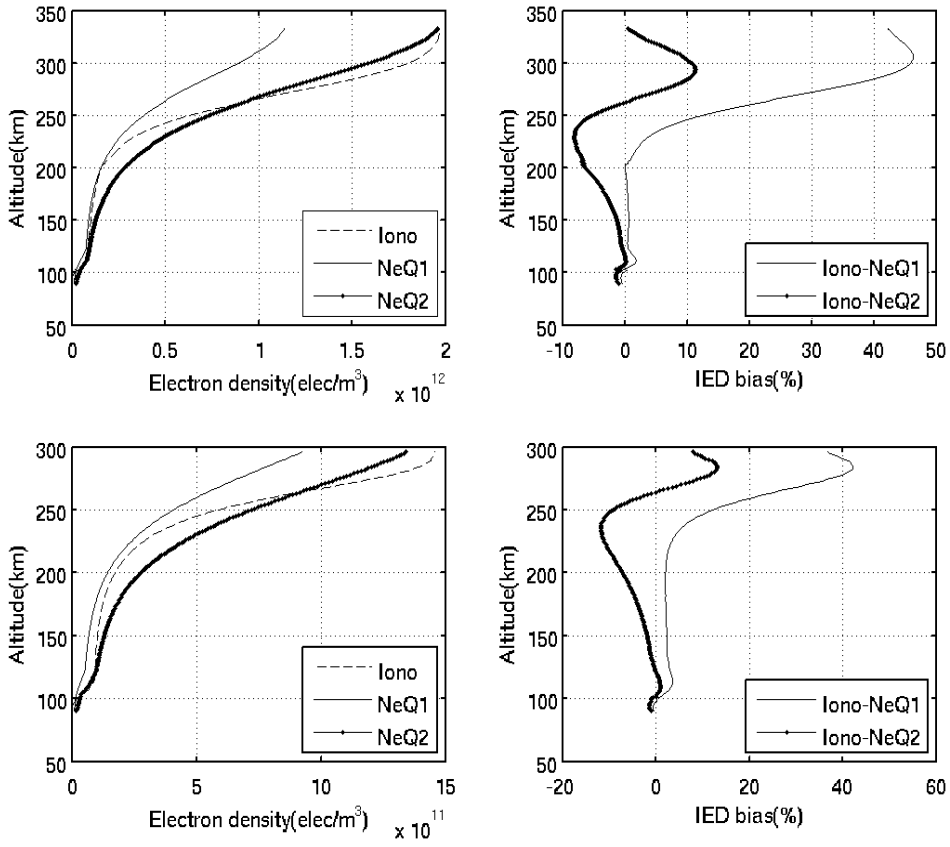

Figure 6.9: A bottomside electron density vertical distribution on May, 2014 at 14:40UT (top two panel) and at 15:00UT (bottom two panel).

Similarly improvement is observed for simulation in June, 2014 at the same time. The June simulation improves from maximum of 70% to maximum of 30% when ionosonde key parameters are used as input to the NeQuick model (see Fig. 6.10).

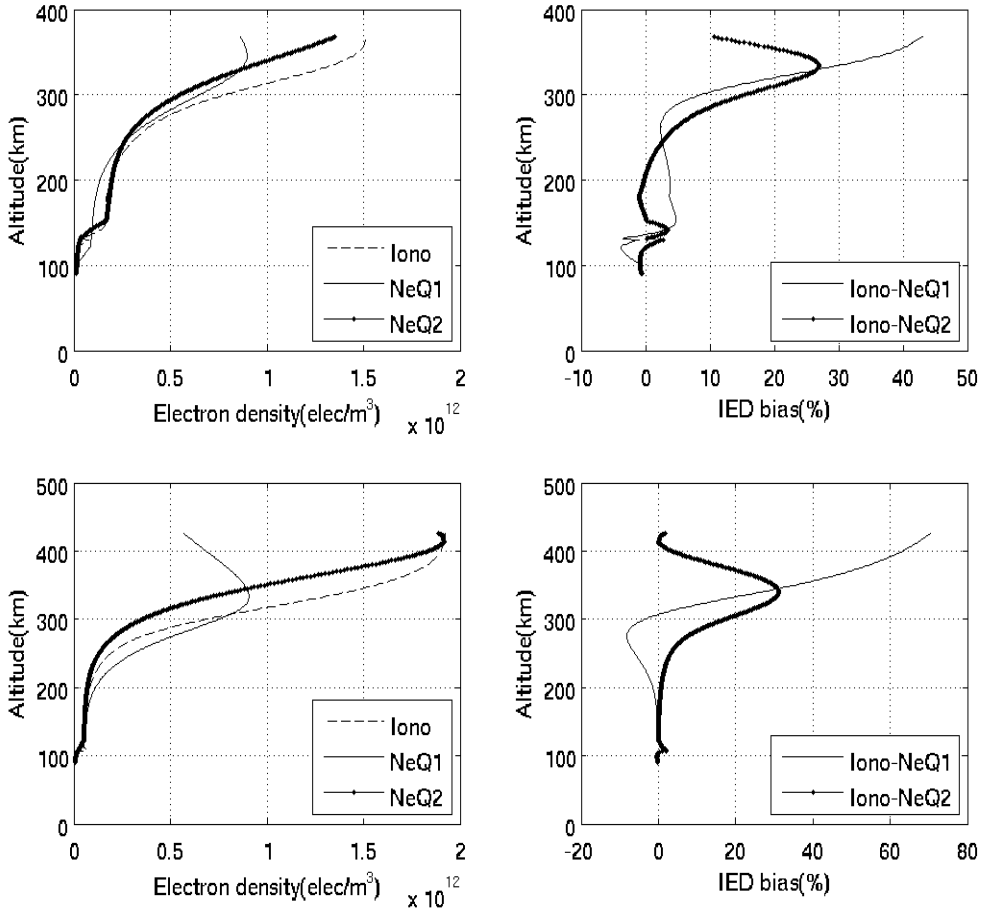

Figure 6.10: A bottomside electron density vertical distribution on June, 2014 at 14:00UT (top two panel) and at 15:05UT (bottom two panel).

The July, 2014 simulation improves from maximum of 60% to maximum of 40% with the use of the ionosonde key parameters as input to the NeQuick model (Fig. 6.11). This shows the electron density structure observed by the ionosonde and simulated by ingesting ionosonde key parameters into NeQuick model show good agreement than NeQuick model without ingesting ionosonde key parameters.

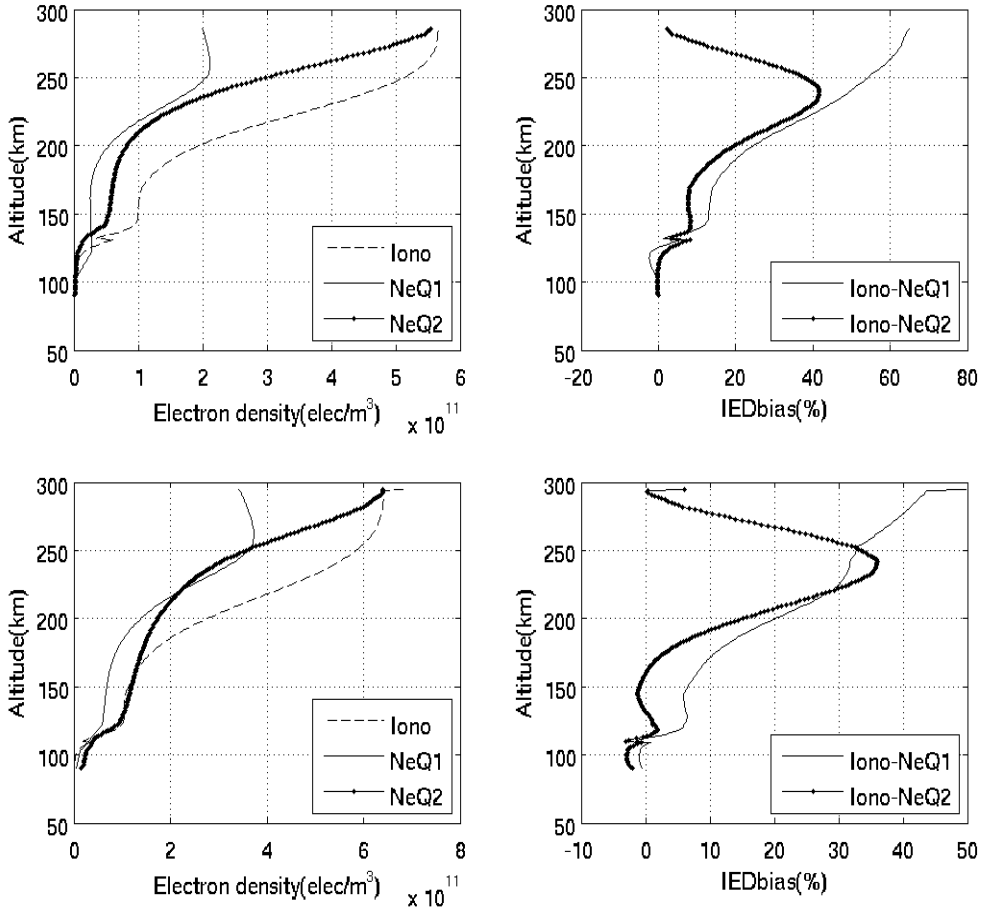

Figure 6.11: A bottomside electron density vertical distribution on July, 2014 at 03:30UT (top two panel) and at 04:00UT (bottom two panel).

The improvements achieved through the use of observed key parameters have also been observed by root mean square deviation and correlation of the simulations with respect to ionosonde electron density observations.

The RMSD and correlation coefficient (R) values were computed for the analysis of both NeQuick model before ingested ionosonde key parameters and NeQuick model after ingested ionosonde key parameter performance as shown in Fig. 6.12 for selected observation time in January, 2012. Fig. 6.12 shows the RMSD and correlation coefficients (R) for both NeQuick model before ingested ionosonde key prameters and NeQuick model after ingested ionosonde key prameters respectively.

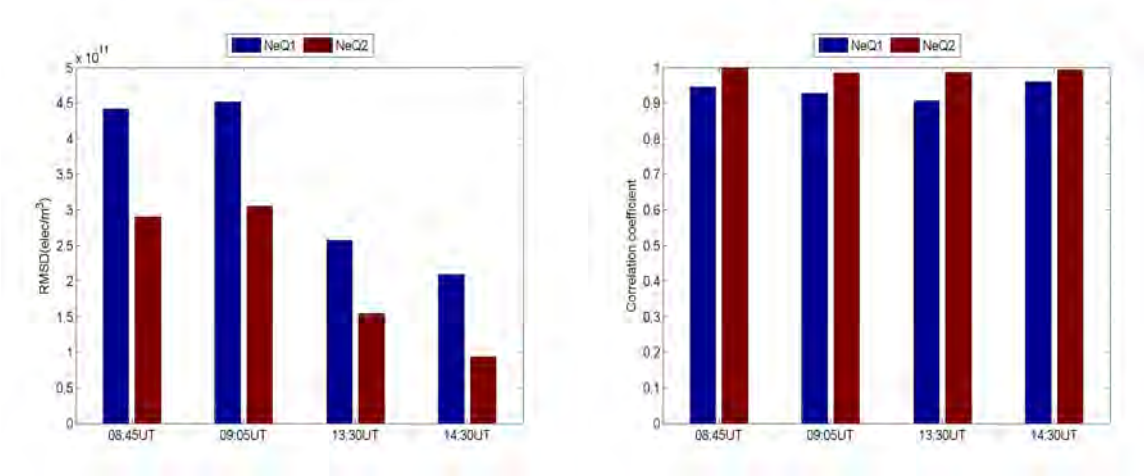

Figure 6.12: The RMSD values (left panel) and correlation coefficients (R) (right panel) of NeQuick model before and after ingested ionosonde key parameters during selected time in January, 2012.

The RMSD is reduced by upto 50% in some cases when ionosonde key parameters are used in NeQuick model. The correlation is also improved substantially from as low as 0.90 to 0.98.

Similarly, simulations in May, 2014 change by the same order of magnitude in RMSD and correlation (Fig. 6.13, top panels). However, the simulations in June, 2014 exhibit wider range of change in RMSD and correlation upon use of ionosonde key parameters. For example, RMSD decreased by a factor of five while correlation improves from a value of 0.69 to 0.99 (Fig. 6.13, bottom panels).

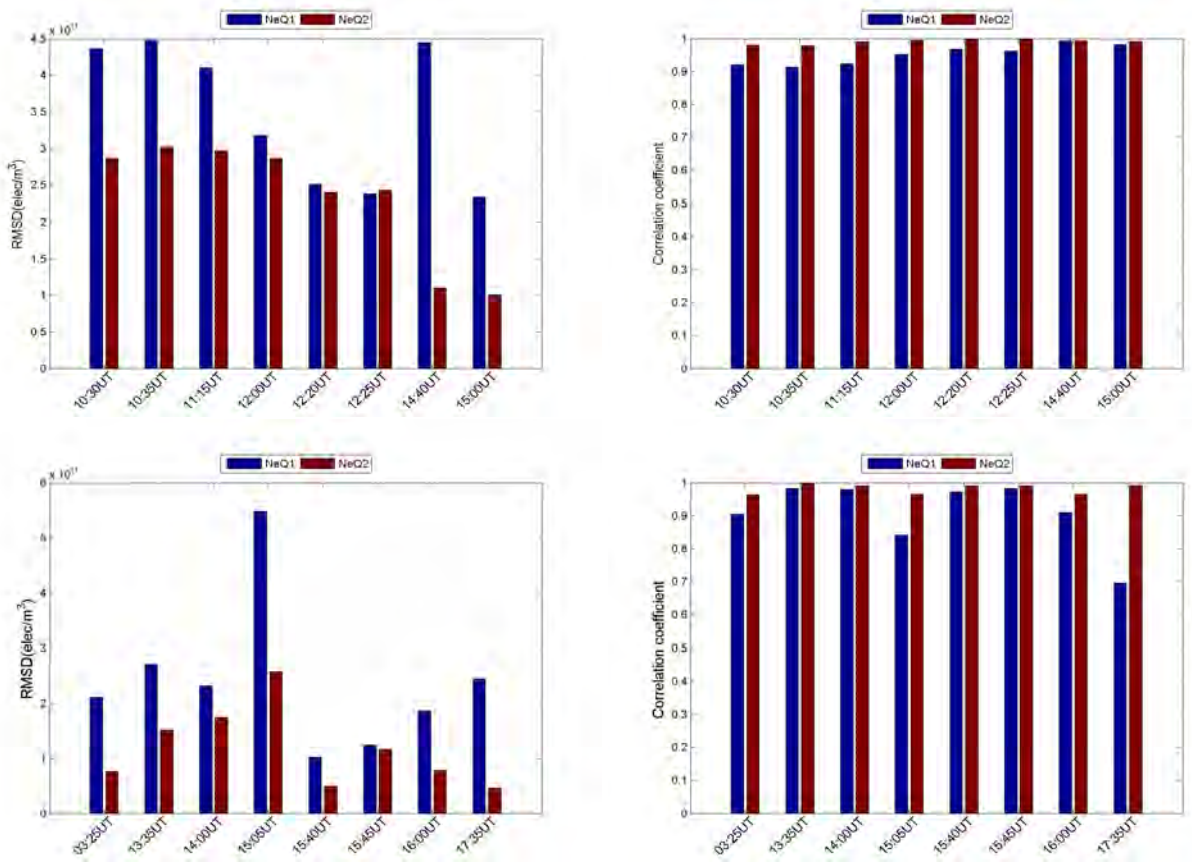

Figure 6.13: A bar graphs of the RMSD values (left panel), and correlation coefficients (R) (right panel) of NeQuick model before and after ingested ionosonde key parameters during selected time in May, 2014 (top two panel) and June, 2014 (bottom two panel).

Chapter 7

Conclusions

The NeQuick ionospheric electron density model over East Africa are validated by the ionosonde data from observations of the newly installed HF-viper radar at Welmera site. Ionosondes can provide measurements of the virtual height via radio reflections that are recorded as ionograms.

The input parameters of the NeQuick model are the position (longitude, latitude and height), the epoch (month and UT) and the solar activity (F10.7 or R12). Other internal parameters are the foE, hmE, foF2 and hmF2 values, which can be obtained from the ionosonde.

The simulated electron density profile from both NeQuick model before and after ingestion of ionosonde key parameters with ionosonde are compared. Comparison results shows that the NeQuick model after ingestion of ionosonde key parameters simulation generally agrees well with ionosonde observations as shown for observations at different times.

The improved simulation results are characterized in terms of bias, RMSD and correlation in electron density with respect to ionosonde observations. The RMSD has improved by a factor of upto five when key parameters from ionosonde is used instead of climatological values. The correlation changes from as low as 0.7 to about 1.

The bias, RMSD and correlation have been evaluated for observations at different time of the day. The observed changes in the above statistics consistantly show improvement across different times.

In general, the performance of the NeQuick model can be improved with the use of key parameters observed by ionosonde. The enhancement in performance in NeQuick model is slightly weaker during disturbed ionosphere than quiet time ionoshere as demonstrated by difference in the performance in January, 2012 and May-July, 2014.

Bibliography

[1] Michael C. Kelley (2009), *The Earths Ionosphere Plasma Physics and Electrodynamics*, International Geophysics Series, Academic Press,inc.

[2] Margaret G.Kilvson and Kristopher T.Russell (1995), *Introduction to Space Physics*, Cambridge University Press.

[3] John S. Seybold (2005), *Introduction to RF propagation*, John Wiley & Sons inc.

[4] Di Giovanni and S. M. Radicella (1990), An analytical model of the electron density profile in the ionosphere, Advances in Space Research, Vol. 10, No. 11, PP. 2730.

[5] Attila Komjathy (1997), Global Ionospheric Total Electron Content Mapping Using the Global Positioning System, PhD Dissertation, University of New Brunswick, Canada.

[6] Y. Kamide and A. Chian (Eds.) (2007), *Handbook of the Solar-Terrestrial Environment*, Springer.

[7] McNamara, L. F (1991), The ionosphere: communications, surveillance, and direction finding, Krieger.

[8] Bonnet, R. M. and Woltjer, L (2008), Surviving 1000 Centuries: Can We Do It?, Praxis.

[9] Ondoh, T. and Marubashi, K (2001), Science of space environment, IOS Press.

[10] R. D. Hunsucker and J. K. Hargreaves (2003), *The High Latitude Ionosphere and its Effect on Radio Propagation*, Cambridge University Press.

[11] Robert W. Schunk and Andrew F. Nagy (2009), *Ionospheres Physics, Plasma Physics, and Chemistry Second Edition.*

[12] Davies K. (1989), Ionospheric Radio (Ionospheric Radio Wave Propagation), Boulder, Colorado.

[13] K. Davies (1989), Ionospheric Radio, radio waves Propagation of effects on ionosphere. Peter peregrinnes Ltd., Lonodon, United Kingdom.

[14] ITU-R (2005), "Ionospheric propagation data and prediction methods required for the design of satellite services and systems". Rec. ITU-R P.531-8, http://lib.convdocs.org/docs/index-2305.html.

[15] ITU-R NeQuick Software for ITU-R Rec. P 531-8, 2002 [Online]. Available: http://www.itu.int/ITU-R/study- groups/software/rsg3-p531-electron-density.zip

[16] Radicella, S. M., Leitinger, R (2001), "The evolution of the DGR approach to model electron density profiles". Adv. Space Res., Vol. 27, No. 1, p. 35-40.

[17] The 10th Generation International Geomagnetic Reference Field, [Online], Available:http://www.ngdc.noaa.gov/IAGA/vmod/igrf.html

[18] Corrected Geomagnetic Coordinates,[Online], Available:http://modelweb.gsfc. nasa.gov/models/cgm/cgmm_des.html

[19] S. M. Radicella and R. Lietinger (2001), The Evolution of the DGR approach to model electron density profiles. Adv, space Res., 27:3540.

[20] S. M. Radicella and M. L. Zhang (1995), The Improved DGR analytical model of electron density height profile and total electron content in the ionosphere.Ann. Geophys., 1:3541.

[21] B. Nava, P. Coisson, G. M. Amarante, F. Aziplicueta, and S. M. Radicella (2005), A model assisted reconstraction method based on verical TEC data ingestion. Annals of Geophysics, 42 (2):107119.

[22] B. Nava, P. Coisson, and S. M. Radicella (2008), A new version of NeQuick ionosphere electron density model. J.Atmos. Sol.Terr. phys., 70:18561862.

[23] P. Coisson, S.M Radicella, R. Leitinger, and B. Nava (2006), Topside electron density in iri and nequick: Features and limitations. ann. Geophys., 37:937942.

[24] Ciraolo, L., Azpilicueta, F., Brunini, C., Meza, A., Radicella, S. M (2006), Calibration errors on experimental slant total electron content (TEC) determined with GPS, Journal of Geodesy, Online Article, September.

[25] Hochegger, G., Nava, B., Radicella, S. M. et al (2000), "A Family of Ionospheric Models for Different Uses". Phys. Chem. Earth (C), Vol. 25, No. 4, p. 307-310.

[26] Rawer, K (1983), "Replacement of the present sub-peak plasma density profile by a unique expression". Adv. Space Res., Vol. 2, No. 10, p. 183-190.

[27] Mosert de Gonzalez, M., Radicella, S. M. (1987), "An empirical model of the F1 intermediate layer true-height characteristics". Adv. Space Res., Vol. 7, No. 6, p. 65-68.

[28] G. Mengistu Tsidua, Gebregiorgis Abraha (2014), Moderate geomagnetic storms of January 22-25, 2012 and their influences on the wave components in ionosphere and MLT. Adv. Space Res., Vol. 54, issue 9, P, 1793-1812, DOI: 10.1016/j.asr. 2014.07.029.

Declaration

This thesis is my original work, has not been presented for a degree in any other University and that all the sources of material used for the thesis have been dully acknowledged.

Name: Kebede Bekele Mamo

Signature:

Place and time of submission: Addis Ababa University, June 2015

This thesis has been submitted for examination with my approval as University advisor.

Name: Prof. Gizaw Mengistu Tsidu
(Botswana International University of
Science and Technology/ Addis Ababa University)

Signature: